Cell Metabolism

Article

Lysosomal lipoprotein processing in endothelial cells stimulates adipose tissue thermogenic adaptation

Graphical abstract

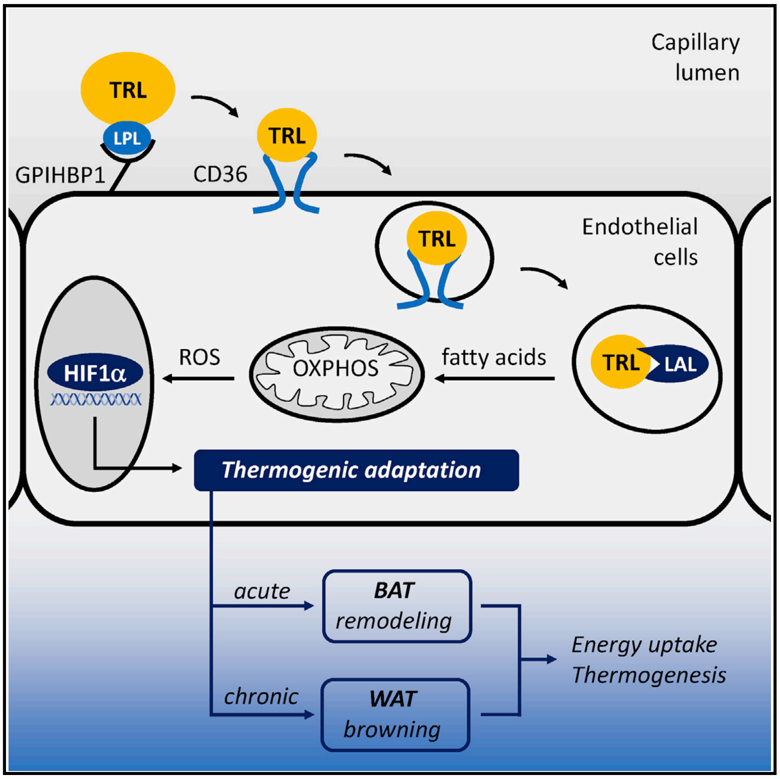

Highlights

- Endothelial cells of cold-activated BAT and WAT endocytose lipoprotein particles
- These triglyceride-rich lipoproteins are processed by LAL
- Subsequently, HIF1α is activated via fatty-acid oxidation and ROS production
- Endothelial LAL deficiency impairs vascularization and thermogenesis in BAT and WAT

Authors

Alexander W. Fischer,
Michelle Y. Jaeckstein,
Kristina Gottschling, ..., Rudolf Reimer,
Ludger Scheja, Joerg Heeren

Correspondence

heeren@uke.de

In Brief

Fischer et al. reveal that endothelial cells of cold-activated BAT and WAT internalize entire triglyceride-rich lipoprotein particles that are targeted toward lysosomes and processed by lysosomal acid lipase. Then, mitochondrial beta-oxidation leads to ROS-dependent HIF1α activation, which promotes vascular and thermogenic remodeling of adipose tissues.

Fischer et al., 2021, Cell Metabolism *33*, 1–18
March 2, 2021
https://doi.org/10.1016/j.cmet.2020.12.001

CellPress

Please cite this article in press as: Fischer et al., Lysosomal lipoprotein processing in endothelial cells stimulates adipose tissue thermogenic adaptation, Cell Metabolism (2020), https://doi.org/10.1016/j.cmet.2020.12.001

Cell Metabolism

CellPress

Article

Lysosomal lipoprotein processing in endothelial cells stimulates adipose tissue thermogenic adaptation

Alexander W. Fischer,[1,2,3,12] Michelle Y. Jaeckstein,[1,12] Kristina Gottschling,[1] Markus Heine,[1] Frederike Sass,[1] Nils Mangels,[1] Christian Schlein,[1] Anna Worthmann,[1] Oliver T. Bruns,[4] Yucheng Yuan,[5] Hua Zhu,[5] Ou Chen,[5] Harald Ittrich,[6] Stefan K. Nilsson,[7] Patrik Stefanicka,[8] Jozef Ukropec,[9] Miroslav Balaz,[10] Hua Dong,[10] Wenfei Sun,[10] Rudolf Reimer,[11] Ludger Scheja,[1] and Joerg Heeren[1,13,*]

[1]Department of Biochemistry and Molecular Cell Biology, University Medical Center Hamburg-Eppendorf, Hamburg, Germany
[2]Department of Molecular Metabolism, Harvard T. H. Chan School of Public Health, Boston, MA, USA
[3]Department of Cell Biology, Harvard Medical School, Boston, MA, USA
[4]Helmholtz Pioneer Campus, Helmholtz Zentrum München, Neuherberg, Germany
[5]Department of Chemistry, Brown University, Providence, RI, USA
[6]Department of Diagnostic and Interventional Radiology, University Medical Center Hamburg-Eppendorf, Hamburg, Germany
[7]Department of Medical Biosciences, Umeå University, Umeå, Sweden
[8]Department of Otorhinolaryngology – Head and Neck Surgery, Comenius University, Bratislava, Slovakia
[9]Institute of Experimental Endocrinology, Biomedical Research Center at the Slovak Academy of Sciences, Bratislava, Slovakia
[10]Institute of Food, Nutrition and Health, ETH Zürich, Schwerzenbach, Switzerland
[11]Heinrich Pette Institute, Leibniz Institute for Experimental Virology, Hamburg, Germany
[12]These authors contributed equally
[13]Lead Contact
*Correspondence: heeren@uke.de

https://doi.org/10.1016/j.cmet.2020.12.001

Summary

In response to cold exposure, thermogenic adipocytes internalize large amounts of fatty acids after lipoprotein lipase-mediated hydrolysis of triglyceride-rich lipoproteins (TRL) in the capillary lumen of brown adipose tissue (BAT) and white adipose tissue (WAT). Here, we show that in cold-exposed mice, vascular endothelial cells in adipose tissues endocytose substantial amounts of entire TRL particles. These lipoproteins subsequently follow the endosomal-lysosomal pathway, where they undergo lysosomal acid lipase (LAL)-mediated processing. Endothelial cell-specific LAL deficiency results in impaired thermogenic capacity as a consequence of reduced recruitment of brown and brite/beige adipocytes. Mechanistically, TRL processing by LAL induces proliferation of endothelial cells and adipocyte precursors via beta-oxidation-dependent production of reactive oxygen species, which in turn stimulates hypoxia-inducible factor-1α-dependent proliferative responses. In conclusion, this study demonstrates a physiological role for TRL particle uptake into BAT and WAT and establishes endothelial lipoprotein processing as an important determinant of adipose tissue remodeling during thermogenic adaptation.

Introduction

Brown adipose tissue (BAT)-dependent nonshivering thermogenesis is a key determinant of energy expenditure in mice. In BAT, heat is generated through release of the proton-motive force across the inner mitochondrial membrane via uncoupling protein 1 (UCP1) (Cannon and Nedergaard, 2004). In addition to classical BAT, cold-induced UCP1-positive cells can also be recruited in white adipose tissue (WAT), a process known as browning. These brite (Petrovic et al., 2008) or beige (Wu et al., 2012) adipocytes are thermogenically active (Shabalina et al., 2013) and can beneficially affect metabolic health in mice (Bartelt and Heeren, 2014).

Heat production by thermogenic adipocytes is mainly dependent on beta-oxidation of fatty acids that are released from intracellular lipid droplets (Young and Zechner, 2013). To replenish lipid stores, activated thermogenic adipocytes take up substantial amounts of nonesterified fatty acids (Furler et al., 2000; Heine et al., 2018), glucose (Heine et al., 2018; Stanford et al., 2013), as well as triglycerides that are delivered by very-low-density lipoproteins (VLDL) and chylomicrons (Bartelt et al., 2011; Dijk et al., 2015; Heine et al., 2018). These triglyceride-rich lipoproteins (TRL) are processed by lipoprotein lipase (LPL) in the vascular lumen, liberating fatty acids that are taken up via transporters such as CD36 and fatty acid-transport protein 1 (Bartelt et al., 2011; Goldberg et al., 2009; Lynes et al., 2017). In

Please cite this article in press as: Fischer et al., Lysosomal lipoprotein processing in endothelial cells stimulates adipose tissue thermogenic adaptation, Cell Metabolism (2020), https://doi.org/10.1016/j.cmet.2020.12.001

consequence, thermogenic activation of adipose tissues lowers plasma triglycerides (Bartelt et al., 2011), accelerates the metabolism of cholesterol-rich lipoproteins (Bartelt et al., 2017; Worthmann et al., 2017), and ultimately reduces atherosclerosis (Berbée et al., 2015). The remaining TRL remnants are internalized by hepatocytes, where lipoprotein-associated triglycerides and cholesterol esters are degraded by lysosomal acid lipase (LAL). The lack of LAL activity results in severe multiorgan lipid-storage disease with premature death in mice and humans (Li and Zhang, 2019). LAL-deficient mice are characterized by steatohepatitis and concomitant lipid depletion in adipose tissues (Du et al., 2001), which is associated with impaired BAT-dependent thermogenesis (Duta-Mare et al., 2018). However, the mechanisms underlying LAL-dependent adipose tissue functions are difficult to dissect since the liver—heavily damaged in global knockouts—has a fundamental role both in maintaining glucose and lipoprotein plasma levels and in the regulation of lipoprotein processing in adipose tissues, heart, and muscle (Scheja and Heeren, 2016). Of note, we previously showed that thermogenically activated BAT and WAT internalize entire TRL particles (Bartelt et al., 2011; Heine et al., 2018; Schlein et al., 2016) in a process that does not depend on low-density lipoproteins (LDL) receptors or apolipoprotein E (Bartelt et al., 2011). Since fatty acids liberated from TRL by LPL and from lipid droplets by intracellular lipases probably provide sufficient energy for mitochondrial respiration (Young and Zechner, 2013), the physiological relevance of the observed lipoprotein particle uptake and subsequent intracellular processing by thermogenic adipose tissues needs to be established.

Thermogenic adipose tissues are highly vascularized to permit efficient flux of energy substrates, oxygen, and heat. Capillary endothelial cells of BAT and WAT form a nonfenestrated vascular endothelium, and thus—probably in an interplay with adipocytes—they are a gatekeeper for nutrient uptake. This concept has been demonstrated for the TRL pathway. Here, GPI-anchored HDL-binding protein 1 (GPIHBP1), a receptor expressed exclusively in endothelial cells, is essential for transendothelial transport of LPL produced in adipocytes (Young et al., 2019). Accordingly, GPIHBP1-deficient mice and humans display massive hypertriglyceridemia (Beigneux et al., 2007; Beigneux et al., 2009). These mice also display cold intolerance (Larsson et al., 2018), emphasizing the importance of endothelial cells for lipid transport and thermogenesis by BAT and WAT. In addition to their role in the control of nutrient uptake, endothelial cells are also mandatory for adipose tissue development and growth (Han et al., 2011; Tran et al., 2012). Cold exposure induces the expansion of thermogenic adipose tissues, which is accompanied by angiogenesis required to maintain functional capacity of BAT and thermogenic WAT (Luo et al., 2017; Xue et al., 2009). Generally, angiogenesis is triggered by the activation of hypoxia-inducible factor 1 alpha (HIF1α), which induces expression of several genes, including vascular endothelial growth factor (*Vegf*) (Li et al., 2019b). This angiogenic factor is expressed by adipocytes in response to cold exposure, adrenergic stimulation (Asano et al., 1997; Fredriksson et al., 2005), or by pharmacological activation of peroxisome proliferator-activated receptor γ (PPARγ) by rosiglitazone (Gealekman et al., 2008). This PPARγ agonist is a known inducer of brite/beige adipocytes in WAT (Ohno et al., 2012; Petrovic et al., 2010). Taken together, these findings suggest that rosiglitazone-dependent browning is at least in part secondary to angiogenesis. By binding to its receptor VEGFR2, VEGF induces proliferation of endothelial cells and sustains angiogenesis (Cao, 2009; Corvera and Gealekman, 2014). Intriguingly, modulation of these pathways has been shown to affect the thermogenic capacity of adipose tissues. Transgenic expression of dominant negative HIF1α (Zhang et al., 2010) and VEGFR2 blockade reduce thermogenic activation (Seki et al., 2016; Wang et al., 2017; Xue et al., 2009). On the other hand, overexpression of VEGF protects from diet-induced obesity by increasing the number of active brown and brite/beige adipocytes (Elias et al., 2012; Park et al., 2017; Sun et al., 2012; Sung et al., 2013), underlining the importance of endothelial cell expansion for thermogenic adaptation of adipose tissues.

Here, we show that endothelial cells of BAT and WAT internalize entire TRL particles, which follow the endosomal pathway for LAL-dependent hydrolysis. Furthermore, utilizing transgenic mice lacking LAL specifically in endothelial cells, we find that intracellular TRL processing is important for cold-induced recruitment of brite/beige adipocytes and adaptive thermogenesis. Mechanistically, we demonstrate that endocytic TRL uptake and subsequent LAL-dependent processing induce proliferation and differentiation of endothelial cells and adipocyte precursors in a HIF-dependent manner. Overall, this study provides evidence for a role of intracellular TRL processing by vascular endothelial cells in the adaptive expansion of thermogenic adipose tissue in response to cold exposure.

Results

Cold exposure induces TRL uptake and the expression of lipoprotein-processing genes in vascular endothelial cells of BAT

To follow the processing of TRL *in vivo*, we used a nanoparticle-based lipoprotein-labeling method (Bruns et al., 2009, 2017) that can employ either quantum dots (QD) for intravital microscopy or superparamagnetic iron-oxide nanoparticles (SPIOs) for magnetic resonance imaging (MRI) (Figure S1A). In this study, we determined the cellular fate and processing of TRL particles in BAT of cold-exposed mice. By intravital microscopy, we detected strong fluorescence signals that were associated with the BAT endothelium of cold-housed but not control (warm-housed) mice 5 min after QD-TRL injection (Figure 1A). Whole-mount staining of BAT showed co-localization of QD-TRL with the endothelial cell marker GPIHBP1 (Figure 1B), a finding that was confirmed in an independent experiment using murine TRL containing Cy3-labeled apolipoproteins (Figure S1B). It is well established that in the initial step of intravascular lipolytic processing, TRL particles bind to LPL attached to GPIHBP1 on the endothelial cell surface (Beigneux et al., 2007), a complex that can be dissociated by exogenously administered heparin (Bartelt et al., 2011). To directly assess whether TRL binding at the vascular endothelium is followed by particle internalization, we performed a heparin-release time course experiment using MRI imaging. The association of SPIO-TRL with BAT of cold-exposed mice was inhibited or reversed when heparin was injected prior to or up to 5 min after SPIO-TRL injection (Figure 1C). Heparin treatment had less to no effect on signal intensities at

Please cite this article in press as: Fischer et al., Lysosomal lipoprotein processing in endothelial cells stimulates adipose tissue thermogenic adaptation, Cell Metabolism (2020), https://doi.org/10.1016/j.cmet.2020.12.001

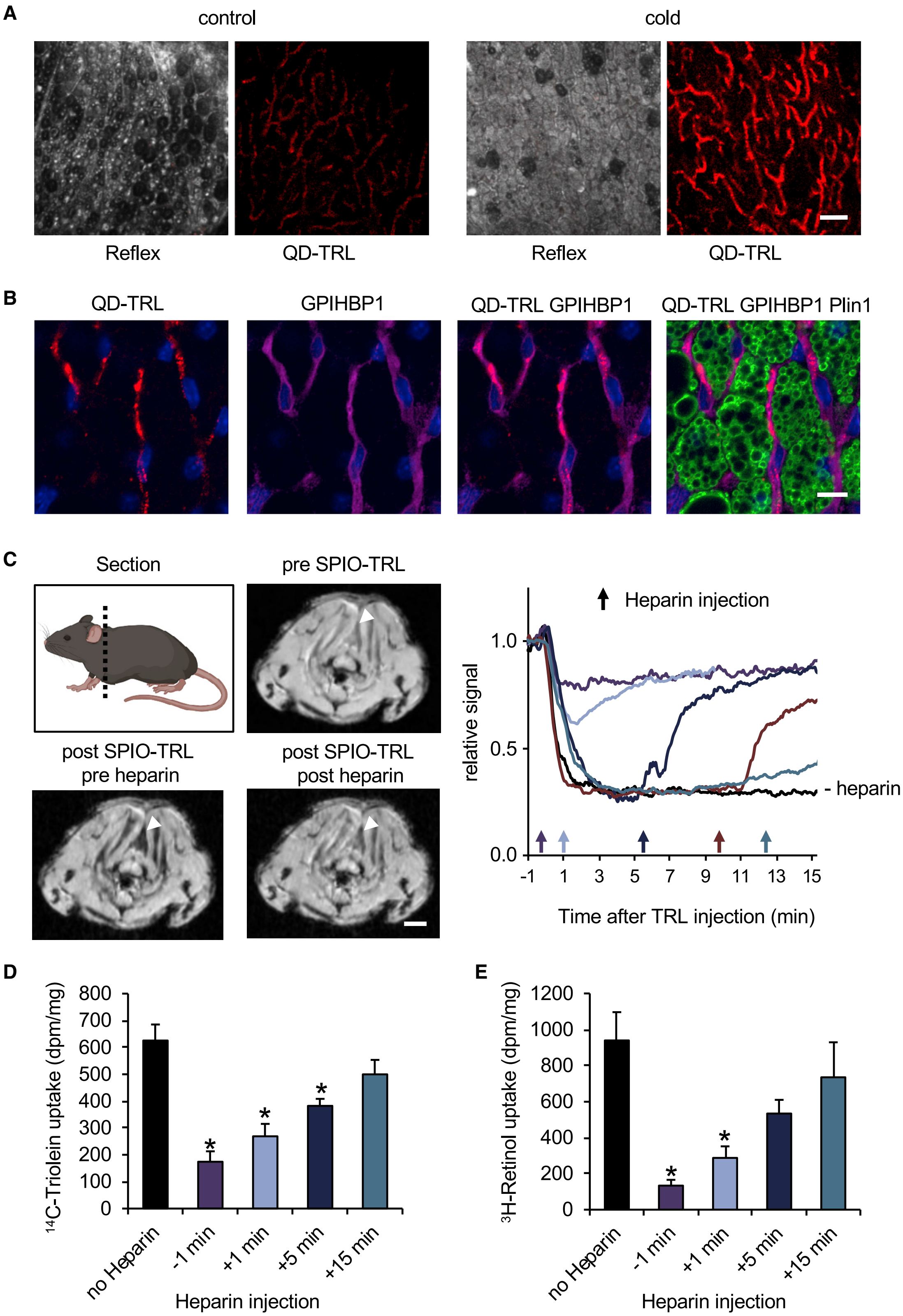

(legend on next page)

Please cite this article in press as: Fischer et al., Lysosomal lipoprotein processing in endothelial cells stimulates adipose tissue thermogenic adaptation, Cell Metabolism (2020), https://doi.org/10.1016/j.cmet.2020.12.001

later time points (Figure 1C). To quantify the effects of heparin treatment before or after TRL injection by an independent approach, we administered TRL particles containing ^{14}C-triolein, a label for both whole particles and fatty acids liberated by lipases, and ^{3}H-retinolester, a label for the particle core (Figures 1D and 1E). Confirming the results generated in the MRI analysis, pretreatment with heparin, as well as treatment up to 5 min post TRL injection diminished the uptake of both fatty acids (Figure 1D) and lipoprotein particles (Figure 1E). However, administration of heparin 15 min after TRL injection had little effect compared with control mice with no heparin treatment (Figures 1D and 1E). These data show that TRLs are inaccessible to heparin at later time points, suggesting that TRLs are internalized by vascular endothelial cells after initial LPL-mediated processing in the lumen of the capillary.

To further explore the processing of TRL by BAT endothelial cells, we determined the expression of genes regulating lipoprotein transport and metabolism, both at the whole organ level (Figure S2A) and in a cell-type-specific manner (Figures 2A–2H). To isolate endothelial cells and adipocytes (Figure 2A), we employed the antibody-based magnetic-activated cell-sorting (MACS®) technology. To avoid potential confounding effects of myeloid cell contamination in the endothelial and adipocyte fractions, we first depleted myeloid cells using anti-CD11b beads (Figure 2A). Successful depletion was verified by qPCR analysis showing high mRNA expression of the macrophage marker *Emr1* in the CD11b+ fraction, while no *Emr1* expression could be detected in the CD31^{+} endothelial cells or in the flow-through (FT) fraction containing predominantly brown adipocytes (Figure S2B). The efficient isolation of endothelial cells was confirmed by high expression of *Gpihbp1* in CD31^{+} cells (Figure 2B). The adipocyte markers *Adipoq* (Figure 2C), *Ucp1* (Figure 2D), and *Glut4* (Figure 2E) were detectable at low levels in CD31^{+} cells but were highly enriched in the FT fraction. As expected, adipocyte genes known to be linked to thermogenesis (*Ucp1*) and energy uptake (*Glut4* and *Lpl*), were higher in cold-exposed compared with control mice (Figures 2D–2F). Of note, basal and cold-induced mRNA levels of the lipid uptake facilitator *Cd36* (Figure 2G) and the gene encoding LAL, *Lipa* (Figure 2H), were higher in the endothelial cell than the FT fraction, indicating that *Cd36* and *Lipa* expression in the CD31^{+} fraction can be explained by endothelial cells rather than contaminating adipocytes.

To validate endothelial expression of lipid- and lipoprotein-handling genes in humans, single nucleus RNA-seq was performed in UCP1-positive BAT biopsies of 16 patients undergoing neck surgery. This dataset has been described and analyzed to deconvolute adipocyte heterogeneity but not to study endothelial cells or genes involved in lipid metabolism (Sun et al., 2020). In this study, we used unsupervised clustering of 40,003 nuclei profiles and identified 12 separate cell clusters (Figure 2I). Among these clusters, mature adipocytes could be detected by expression of ADIPOQ (Figure 2J), whereas endothelial cells were identified by expression of cadherin 5 (CDH5) (Figure 2K). Notably, CD36 was strongly associated with both the adipocyte and endothelial cell clusters (Figure 2L). The majority of LPL expression was detected in mature adipocytes (Figure 2M). LIPA reads were generally low, which may be due to technical limitations of the single-nuclei RNA-seq method, but expression was detected in both endothelial cells and mature adipocytes as well as in other clusters (Figure 2N). Taken together, BAT endothelial cells are equipped for the internalization and lysosomal degradation of TRL.

Endothelial cells of cold-activated BAT internalize whole TRL particles via CD36

To quantify the uptake of TRL-derived fatty acids and TRL particles simultaneously, we double-labeled lipoproteins with ^{14}C-triolein, a label for both whole particles and fatty acids liberated by lipases, and the nonhydrolysable ^{3}H-cholesterol ether for exclusive labeling of the particle core (Figure 3A). After injection of these radiolabeled TRLs in cold-exposed and control mice, we isolated endothelial cells and adipocytes from BAT by MACS® as described above. As indicated by the ^{3}H-cholesterol ether, TRL particles were almost exclusively taken up by endothelial cells and uptake was strongly induced by cold exposure (Figure 3B). A cold-dependent induction was also observed for the fatty acid label ^{14}C-triolein; however, equivalent quantities of the label were detected in endothelial cells and adipocytes (Figure 3C). Similar results were obtained when primary rat chylomicrons double-labeled with ^{3}H-retinol ester as core label (Figure S3A) and ^{14}C-triolein (Figure S3B) were used. This demonstrates that a large fraction of TRL particles is internalized and sequestered by endothelial cells while TRL fatty acids are channeled to adipocytes of cold-activated BAT.

Figure 1. Visualization of lipoprotein particle processing by endothelial cells of activated BAT *in vivo*

Wild-type mice were housed at 22°C (control) or exposed to 6°C (cold) for 24 h.

(A) Intravital imaging was used to visualize TRL processing by interscapular BAT in real time. Representative images taken 5 min after injection of QD-labeled TRL show BAT structure (reflection, gray) and TRL (red). Scale bar, 50 μm.

(B) BAT was harvested 20 min after injection of QD-TRL into cold-exposed mice. Whole-mount staining was performed to visualize nuclei (DAPI, blue), QD-TRL (red), GPIHBP1 (purple), and lipid droplet associated perilipin (green). Scale bar, 10 μm.

(C) Association of SPIO-labeled TRL with interscapular BAT was followed by magnetic resonance imaging in cold-exposed mice. Upper panel: representative transversal sections showing interscapular BAT regions (white arrow) that were used for quantification. Graph: SPIO-TRL were administered, preceded or followed by heparin injections at indicated time points (see color-coded arrows). A decrease in signal indicates association of SPIO-TRL with BAT. The "no heparin control" is indicated separately.

(D and E) Cold-exposed mice were injected with ^{14}C-triolein-^{3}H-retinolester double-labeled TRL, preceded or followed by heparin injections at indicated time points.

(D) BAT uptake of ^{14}C-triolein (n = 4).

(E) BAT uptake of ^{14}C-retinolester (n = 4).

*$p < 0.05$ by one-way ANOVA compared with "no heparin."

See also Figure S1.

Please cite this article in press as: Fischer et al., Lysosomal lipoprotein processing in endothelial cells stimulates adipose tissue thermogenic adaptation, Cell Metabolism (2020), https://doi.org/10.1016/j.cmet.2020.12.001

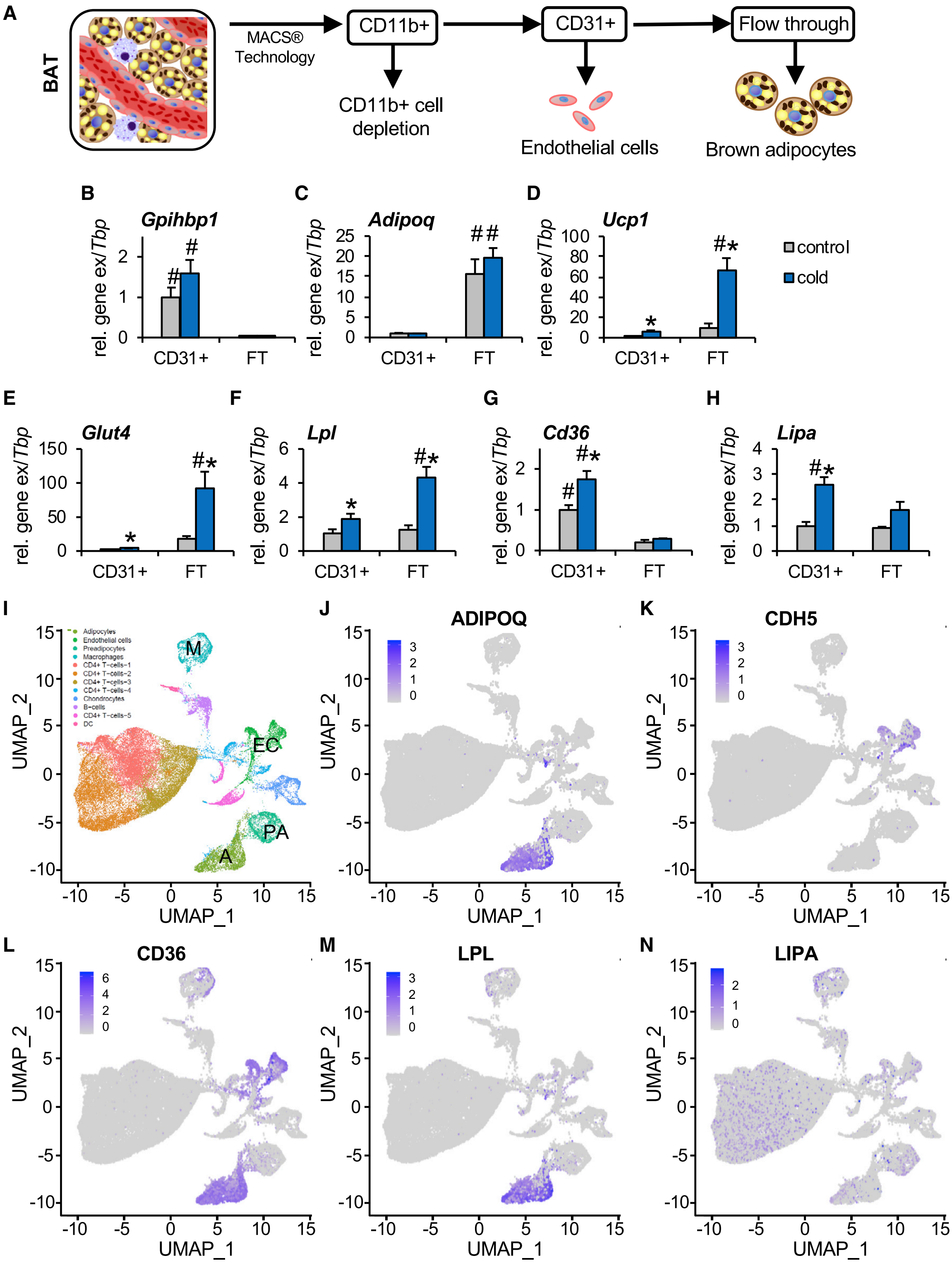

Figure 2. Cell-type-specific expression of lipoprotein-handling genes in murine and human BAT

(A) Picture describing purification of endothelial cells from BAT using MACS® technology.

(B–H) Wild-type mice were housed at 22°C (control) or at 6°C (cold) for 24 h. Gene expression in CD31^{+} endothelial cells and adipocyte-enriched flow-through fraction isolated from BAT of control and cold-exposed mice. Gene expression is presented as mean values ± SEM from up to 13 independent isolations.

(B) Gene expression of *Gpihbp1*.

(C) Gene expression of *Adipoq*.

(legend continued on next page)

Please cite this article in press as: Fischer et al., Lysosomal lipoprotein processing in endothelial cells stimulates adipose tissue thermogenic adaptation, Cell Metabolism (2020), https://doi.org/10.1016/j.cmet.2020.12.001

Lipoprotein particle processing by BAT endothelial cells of cold-exposed mice was further studied by electron microscopy (Figure S3C). After injection of TRL harboring electron-dense SPIOs, initial attachment of TRL particles to the endothelium (Figure 3D, image I), shrinkage indicative of LPL processing at the vascular surface (image II), endothelial TRL particle endocytosis (Figure 3D, image III), and finally SPIO-TRL presence within endosomal structures (Figure 3D, image IV) were observed. To confirm endosomal localization, the superparamagnetic properties of SPIO-TRL were utilized for magnetic pulldown (Figure S3C). Western blot analysis showed enrichment of the lysosomal protein LAMP2 and the endosomal marker RAB5 in the pulldown fractions of BAT from cold-exposed mice (Figure 3E). This was not observed for markers of cytosol, mitochondria, or lipid droplets. The specificity of the pulldown approach was demonstrated by using nonmagnetic QD-TRL as negative controls.

Previously, we have shown that CD36 is important for efficient lipid disposal in activated BAT (Bartelt et al., 2011; Schlein et al., 2016), and it has been demonstrated that CD36 expressed by endothelial cells mediates fatty acid uptake into metabolically active tissues (Son et al., 2018). To study whether CD36 also mediates uptake of whole TRL particles, we first determined CD36 localization within BAT. In line with expression data of isolated cells (Figure 2G), we found a strong induction of CD36 immunostaining in endothelial cells of cold-exposed mice (Figure 3F). Moreover, by an *in vivo* intravascular biotinylation approach, higher levels of CD36 protein were detected in BAT on the endothelial surface of cold-housed versus control mice, while GPIHBP1 presence on the cell surface was unaltered (Figure 3G). These data suggest that next to *Cd36* expression, translocation of CD36 to the endothelial plasma membrane is also increased. Notably, the cold-induced *in vivo* uptake of whole particles and fatty acids into endothelial cells and the shuttling of fatty acids into adipocytes was blunted in CD36-deficient mice (Figures 3H and 3I). This was reflected by a lack of cold-induced uptake of both whole particles and fatty acids in CD36-deficient BAT on a whole-tissue level (Figures 3J and 3K). These data were confirmed by electron microscopy studies (Figures S3D and S3E). In wild-type but not CD36-deficient mice, we observed engulfment of TRL particles by endothelial cells only after considerable shrinkage, the latter indicated by the small size of the internalized particles and the dense packaging of the SPIOs. Taken together, these findings show that TRL particles are first processed by triglyceride hydrolysis in the vascular lumen, internalized in a CD36-dependent manner, and eventually targeted to the endosomal/lysosomal compartment of BAT endothelial cells.

Endothelial cell-specific deletion of LAL results in impaired thermogenesis

LAL is the only hydrolytic lysosomal enzyme for triglycerides and cholesterol esters of endocytosed lipoproteins (Li and Zhang, 2019); therefore, blocking the enzyme in endothelial cells allows us to study the relevance of TRL particle uptake into these cells for the function of thermogenic adipose tissues. In this study, we crossed mice expressing a tamoxifen-inducible Cre recombinase under the control of the VE-cadherin (Cdh5) promoter with *Lipa*$^{flox/flox}$ mice to generate mice lacking LAL in endothelial cells (*Lipa*$^{fl/fl}$-Cdh5^{Cre+}) and control littermates (*Lipa*$^{fl/fl}$-Cdh5^{Cre-}), which were both treated with tamoxifen. The inducible gene knockout was demonstrated by recombination-specific PCR in BAT of *Lipa*$^{fl/fl}$-Cdh5^{Cre+} but not in *Lipa*$^{fl/fl}$-Cdh5^{Cre-} (Figure S4A). Confirming cell-type-specific deletion, *Lipa* expression was reduced in MACS®-isolated endothelial cells but not in adipocytes of BAT and inguinal WAT from control-housed *Lipa*$^{fl/fl}$-Cdh5^{Cre+} mice (Figures S4B and S4C). For metabolic phenotyping, transgenic mice were fed with a cholesterol-enriched high-fat diet, which better reflects typical human diets compared with sugar- and fiber-rich rodent-chow diets and enhances lipoprotein particle uptake and processing by murine adipose tissues. To account for differences in the basal thermogenic differentiation states (Kalinovich et al., 2017), we utilized two different cold-exposure regimens to study acclimation processes, namely, 4 days acute cold exposure with the focus on BAT, and 4 weeks of chronic cold for WAT browning. Following acute cold exposure, *Lipa*$^{fl/fl}$-Cdh5^{Cre+} mice presented a reduction in whole-body energy expenditure (Figures 4A and 4B). Energy intake and physical activity were not different (Figures S4D and S4E), while a trend toward lower body temperature was detected in *Lipa*$^{fl/fl}$-Cdh5^{Cre+} mice (Figure S4F). The latter, however, is not a direct readout for BAT activity but suggests a general impairment in responding properly to cold environments in these mice. Lipid and glucose uptake into BAT (Figure 4C) but not into inguinal WAT (Figure S4G) were reduced in *Lipa*$^{fl/fl}$-Cdh5^{Cre+} versus *Lipa*$^{fl/fl}$-Cdh5^{Cre-} mice. Consistently, gene expression of thermogenic marker genes (Figure 4D), as well as total UCP1 protein levels (Figures 4E and 4F) were reduced in BAT of *Lipa*$^{fl/fl}$-Cdh5^{Cre+} versus *Lipa*$^{fl/fl}$-Cdh5^{Cre-} mice. Altogether, these data indicate that LAL in endothelial cells is important for proper adaptation of BAT in response to acute cold.

(D) Gene expression of *Ucp1*.
(E) Gene expression of *Glut4*.
(F) Gene expression of *Lpl*.
(G) Gene expression of *CD36*.
(H) Gene expression of *Lipa*.
(I–N) Single nucleus RNA sequencing of 40,003 nuclei of deep-neck BAT of 16 individuals.
(I) Unsupervised clustering and annotation plot by SingleR. A, adipocytes; EC, endothelial cells; M, macrophages; PA, preadipocytes.
(J) Feature plot for ADIPOQ.
(K) Feature plot for CDH5.
(L) Feature plot for CD36.
(M) Feature plot for LPL.
(N) Feature plot for LIPA.
*p < 0.05 by two-way ANOVA comparing control versus cold. #p < 0.05 by two-way ANOVA comparing CD31$^+$ cells versus FT. See also Figure S2.

Please cite this article in press as: Fischer et al., Lysosomal lipoprotein processing in endothelial cells stimulates adipose tissue thermogenic adaptation, Cell Metabolism (2020), https://doi.org/10.1016/j.cmet.2020.12.001

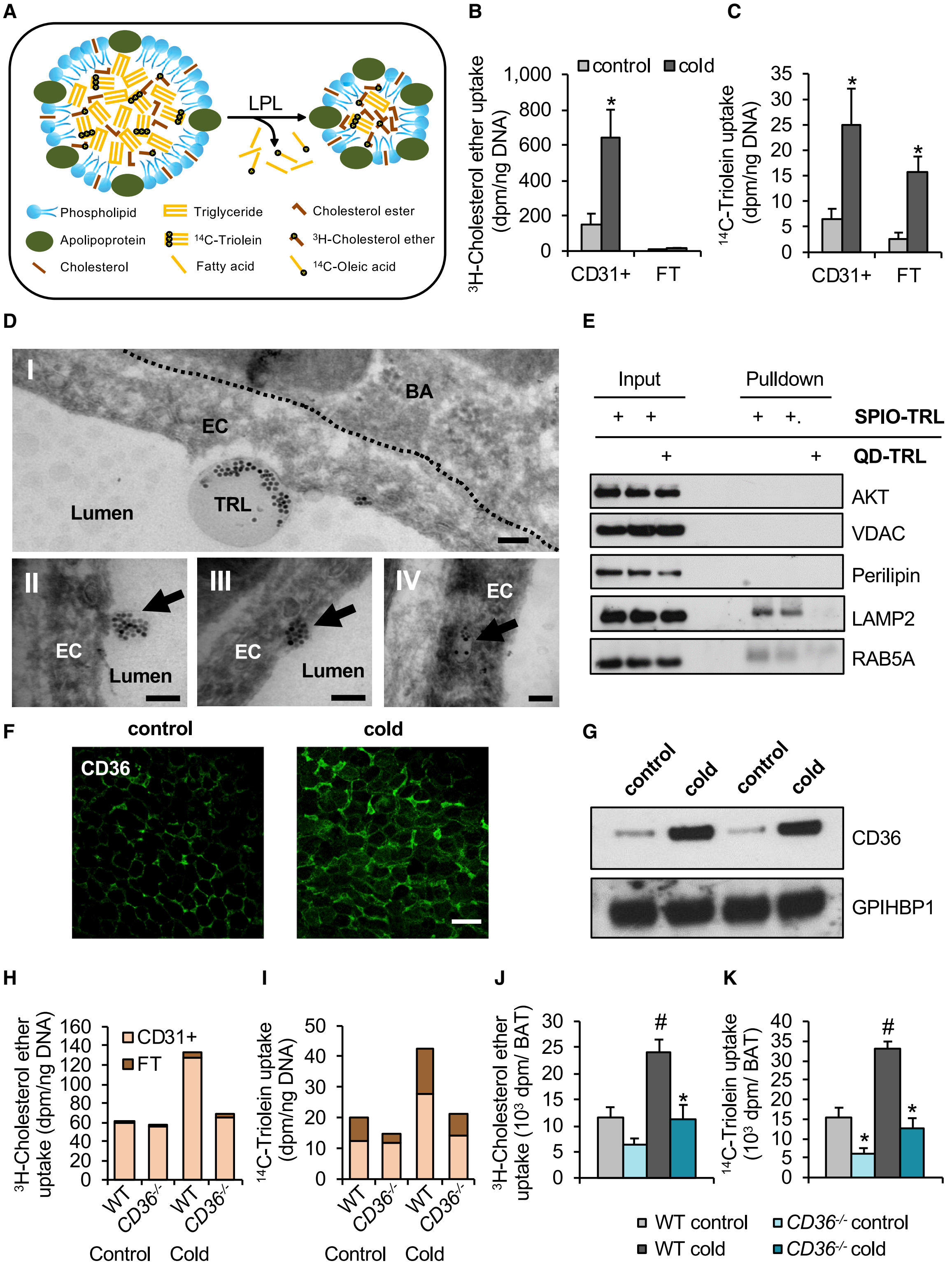

Figure 3. Endothelial cells of activated BAT internalize and sequester whole TRL particles via CD36

(A) Schematic drawing showing TRL labeling with ^{3}H-cholesterol ether (CEt) and ^{14}C-triolein, allowing to follow the fate of the particle core or fatty acids liberated by LPL.

(B–G) BAT was harvested from wild-type mice housed at room temperature (control) or at 6°C for 24 h (cold). For uptake studies, BAT was harvested 20 min after injection of labeled TRL.

(B) Uptake of ^{3}H-CEt into MACS®-isolated endothelial cells (CD31$^+$) and adipocytes (FT) (n = 5).

(legend continued on next page)

Please cite this article in press as: Fischer et al., Lysosomal lipoprotein processing in endothelial cells stimulates adipose tissue thermogenic adaptation, Cell Metabolism (2020), https://doi.org/10.1016/j.cmet.2020.12.001

Next, we studied transgenic mice under chronic cold conditions to determine the role of endothelial LAL in brite/beige adipose tissues. Gene expression analysis confirmed cell-type-specific knockout of *Lipa* (Figures S4H and S4I). As observed under acute cold, *Lipa*$^{fl/fl}$-Cdh5^{Cre+} mice displayed reduced daytime and diurnal levels of energy expenditure (Figures 4G and 4H). Energy intake and physical activity were unaffected (Figures S4J and S4K), while a trend toward a lower body temperature was observed (Figure S4L). Importantly, as determined by a combined oral-fat and glucose-tolerance test, the total organ uptake of the tracers ^{3}H-deoxyglucose and ^{14}C-triolein was similar in BAT of *Lipa*$^{fl/fl}$-Cdh5^{Cre+} and *Lipa*$^{fl/fl}$-Cdh5^{Cre} mice under these conditions (Figure S4M). In contrast, glucose and lipid uptake was lower in inguinal WAT of mice lacking LAL in endothelial cells (Figure 4I). Moreover, maximal thermogenic capacity determined by indirect calorimetry after the injection of the beta-3-agonist CL316,243 was lower in *Lipa*$^{fl/fl}$-Cdh5^{Cre+} than in *Lipa*$^{fl/fl}$-Cdh5^{Cre-} mice (Figure S4N). This was accompanied by reduced tail temperature, indicative of lower CL316,243-induced heat production (Figure S4O). In line with the reduced nutrient uptake into inguinal WAT, the content of multilocular brite/beige adipocytes (Figure 4J) and the expression of typical thermogenic and mitochondrial genes, including *Ucp1*, *Dio2*, *Cox7a*, and *Elovl3* (Figure 4K), were lower in *Lipa*$^{fl/fl}$-Cdh5^{Cre+} compared with *Lipa*$^{fl/fl}$-Cdh5^{Cre-} mice. In contrast, BAT thermogenic genes were largely unchanged (Figure S4P), and a similar or even higher abundance of BAT thermogenic and mitochondrial proteins was confirmed by western blot (Figures S4Q and S4R). In contrast, proteins enriched in brite/beige versus white adipocytes, such as UCP1, DIO$_2$, as well as mitochondrial oxidative phosphorylation (OXPHOS) proteins were lower in inguinal WAT from *Lipa*$^{fl/fl}$-Cdh5^{Cre+} compared with *Lipa*$^{fl/fl}$-Cdh5^{Cre-} mice (Figures 4L and 4M). Impaired lipid handling in WAT but not in BAT of mice lacking endothelial LAL was reflected by reduced tissue cholesterol-ester content, while the levels of other lipid classes were unchanged (Figures S4S–S4V). Moreover, and in line with a general defect in endothelial cell lipid processing in these mice, we found an accumulation of TRL core label in endothelial cells of BAT and WAT from *Lipa*$^{fl/fl}$-Cdh5^{Cre+} mice compared with *Lipa*$^{fl/fl}$-Cdh5^{Cre-} mice (Figures S4W–S4Z), while whole-tissue uptake was only modestly affected in WAT but not BAT (Figures S4AA and S4AB). Taken together, these data show that LAL in endothelial cells is important for adaptive responses in BAT after acute and in WAT after chronic cold exposure.

LAL modulates abundance of HIF1α and endothelial markers in BAT and WAT

Alterations in endothelial cell proliferation and angiogenesis, prerequisites for adipose tissue expansion and function (Luo et al., 2017; Xue et al., 2009), may explain the impaired cold adaptation of BAT and WAT in the absence of endothelial LAL. In line with this hypothesis, protein expression of the angiogenic transcription factor HIF1α and its target pyruvate dehydrogenase kinase 1 (PDK1) were reduced in BAT (Figures 5A and 5B) but not in inguinal WAT (Figures S5A and S5B) of *Lipa*$^{fl/fl}$-Cdh5^{Cre+} compared with *Lipa*$^{fl/fl}$-Cdh5^{Cre-} mice under conditions of acute cold exposure. Furthermore, the endothelial cell proteins zonula occludens-1 (ZO-1) and epithelial cadherin (CDH1) were reduced in BAT but not in inguinal WAT of the knockout mice (Figures 5A, 5B, S5A, and S5B). This was accompanied by specific reductions in expression levels of *Pdk1* and endothelial markers *Tjp1* (ZO-1) and *Pecam1* (CD31) in BAT (Figure 5C) but not in inguinal WAT of *Lipa*$^{fl/fl}$-Cdh5^{Cre+} mice (Figure S5C). In line with these findings, CD31-positive area in BAT sections of acutely cold-exposed *Lipa*$^{fl/fl}$-Cdh5^{Cre+} was diminished compared with *Lipa*$^{fl/fl}$-Cdh5^{Cre-} mice (Figures 5D and 5E).

Consistent with an effect of endothelial LAL deficiency on WAT browning under conditions of prolonged cold acclimation, the protein levels of HIF1α, PDK1, and the endothelial cell markers ZO-1 and CDH1 were reduced in inguinal WAT (Figures 5F and 5G) but not in BAT (Figures S5D and S5E) of long-term cold-acclimated *Lipa*$^{fl/fl}$-Cdh5^{Cre+} compared with *Lipa*$^{fl/fl}$-Cdh5^{Cre-} mice. Similarly, expression of the angiogenic markers *Cdh5*, *Tjp1*, and *Pecam1* was reduced in inguinal WAT (Figure 5H) but not in BAT (Figure S5F) of *Lipa*$^{fl/fl}$-Cdh5^{Cre+} compared with *Lipa*$^{fl/fl}$-Cdh5^{Cre-} mice. Notably, *Pdk1* and *4* were lower in WAT (Figure 5H), while other HIF1α target genes were unaffected (Figures S5G and S5H). Reduced CD31-positive area in inguinal WAT after chronic cold acclimation confirmed reduced angiogenic responses in *Lipa*$^{fl/fl}$-Cdh5^{Cre+} compared with control mice (Figures 5I and 5J). The lower expression of the HIF1α target genes *Pdk1* and *Pdk 4* as seen on a whole-tissue level was confirmed in endothelial cells isolated by MACS® from

---

Data in (B) and (C) are presented as mean values ± SEM, *p<0.05 by Student's t test comparing control versus cold.

(C) Uptake of ^{14}C-triolein in CD31^{+} cells and FT (n = 5).

(D) Electron microscopy analysis after injection of SPIO-labeled TRLs. Representative images showing different stages of TRL processing: I, attachment; II, shrinkage; III, engulfment; IV, appearance in endosomal compartments. Dotted line represents the border between the brown adipocyte (BA) and the endothelial cell (EC). Scale bar, 100 nm.

(E) Magnetic pulldown of BAT lysates from cold-exposed mice after injection of QD- or SPIO-labeled TRLs. Input fraction (postnuclear lysate) as well as magnetic pulldown fractions were analyzed for markers of cytosol (AKT), lipid droplets (perilipin), mitochondria (VDAC), as well as endosomes (RAB5a) and lysosomes (LAMP2).

(F) Immunostaining of CD36 (green). Scale bar, 50 μm.

(G) After *in vivo* vascular surface biotinylation, BAT lysates were generated for streptavidin pulldown. Western blot of CD36 and GPIHBP1 was performed with pulldown fractions.

(H–K) For uptake studies in *CD36*$^{-/-}$ mice and littermate controls, cold exposure was limited to 4 h to avoid hypothermia in knockouts.

(H) Uptake of ^{3}H-CEt into MACS®-isolated endothelial cells (CD31^{+}) and adipocytes (FT) pooled from n = 6 mice.

(I) Uptake of ^{14}C-triolein in endothelial cells and adipocytes as described in (H).

(J) Uptake of ^{3}H-CEt into BAT.

(K) Uptake of ^{14}C-triolein into BAT of the same mice, as shown in (J).

Data in (J) and (K) are presented as mean values ± SEM (n = 5–6), $^{\#}p < 0.05$ control versus cold, $^{*}p < 0.05$ WT versus *CD36*$^{-/-}$ by two-way ANOVA. See also Figure S3.

Please cite this article in press as: Fischer et al., Lysosomal lipoprotein processing in endothelial cells stimulates adipose tissue thermogenic adaptation, Cell Metabolism (2020), https://doi.org/10.1016/j.cmet.2020.12.001

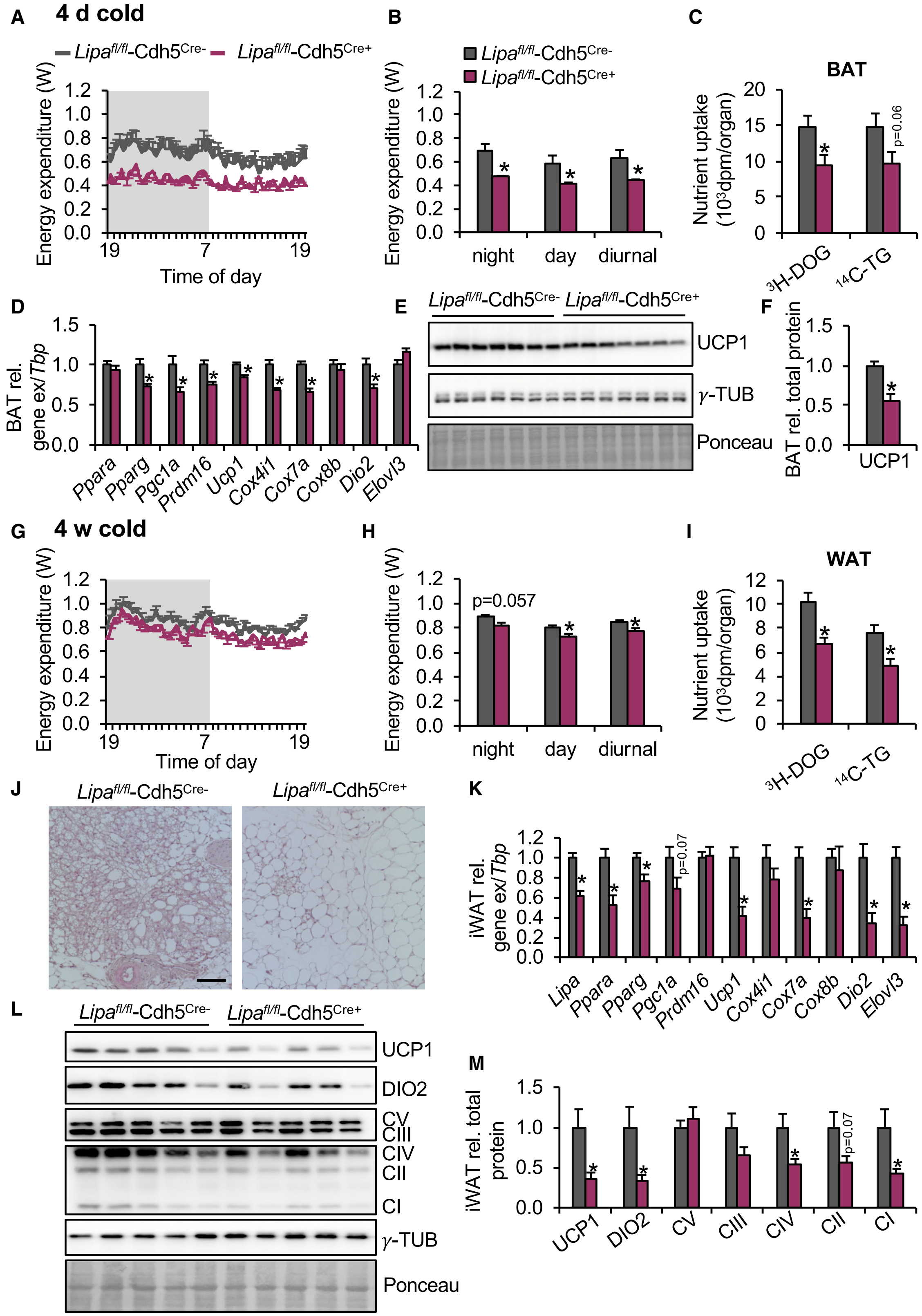

(legend on next page)

inguinal WAT of transgenic mice, where expression of *Pdk1* and *Pdk4* was significantly reduced in *Lipa*$^{fl/fl}$-Cdh5^{Cre+} compared with *Lipa*$^{fl/fl}$-Cdh5^{Cre-} mice (Figure 5K). In the adipocyte-enriched flow through, *Ucp1* expression was markedly reduced (Figure 5L), confirming the browning phenotype. Overall, endothelial LAL enhances HIF1α activity and expression of endothelial cell markers under conditions of thermogenic differentiation in BAT and WAT *in vivo*.

LAL-dependent TRL processing stimulates proliferation and thermogenic differentiation via HIF1α

Reduced abundance of thermogenic adipocytes, lower HIF1α content, and decreased endothelial markers in BAT and WAT of *Lipa*$^{fl/fl}$-Cdh5^{Cre+} indicate that intracellular TRL processing promotes the activation of HIF1α during cold acclimation. To address this hypothesis under defined conditions, we incubated human vascular endothelial cells (HUVEC) with TRL and detected higher protein levels of HIF1α and PDK1 compared with controls, an effect that was blunted by co-incubation with the specific LAL inhibitor Lalistat (Figures S6A and S6B) (Rosenbaum et al., 2010). Next, we investigated these TRL effects in WT1, a precursor cell line for thermogenic adipocytes that was generated by immortalization of stromal-vascular cells from murine BAT (Klein et al., 1999). In these precursor cells, the TRL effects mediated by LAL on HIF1α activity were even more pronounced than those observed in HUVEC (Figures 6A–6C). To study a causal role of HIF1α, we employed a specific inhibitor that suppresses induction of the transcription factor in cells cultured under hypoxic conditions (Figure S6C). Notably, HIF1α induction and expression of its targets in response to TRL treatment were also blunted by this inhibitor (Figures 6D–6F), confirming a causal role of HIF1α in TRL-triggered signaling. The upregulation of HIF1α and its target genes *Pdk1* and *Pdk4* that trigger a metabolic response associated with cell growth (Wang et al., 2019; Woolbright et al., 2018) prompted us to investigate a potential effect of TRL on cellular proliferation. As determined by ^{3}H-thymidine incorporation, TRL treatment promoted proliferation of HUVEC and WT1 cells, and this effect was blunted by LAL inhibition using Lalistat (Figures S6D and S6E). Furthermore, TRL-dependent proliferation was prevented by the HIF1α inhibitor (Figures S6F and S6G). Altogether, these data indicate that the degradation of internalized TRL particles by LAL triggers HIF1α-dependent signaling and proliferation. A possible link between lysosomal lipid processing and HIF1α activation could be related to the catabolism of fatty acids released by the action of LAL. Interestingly, incubation of WT1 preadipocytes with TRL led to a LAL-dependent increase in the generation of reactive oxygen species (ROS) (Figure S6H). ROSs have previously been linked to HIF1α stabilization (Jung et al., 2008; Movafagh et al., 2015), and we thus examined whether fatty acid metabolism and ROS production link LAL-mediated TRL processing with HIF1α activity. To this end, we treated WT1 cells with TRL and etomoxir, an inhibitor of mitochondrial fatty acid import and beta-oxidation. Similar to the effects of LAL and HIF1α inhibition, etomoxir treatment abolished the effects of TRL treatment on HIF1α activity (Figures 6G–6I). Similarly, reducing intracellular ROS levels with the mitochondrial antioxidant MitoQ also led to a blunted induction of HIF1α levels and target gene expression (Figures 6J–6L). Taken together, these data indicate that lysosomal TRL processing leads to release of fatty acids that increase ROS production, and thereby affect HIF1α activity and proliferation.

To elucidate whether LAL- and HIF1α-dependent effects of TRLs on proliferation would also translate into altered thermogenic adipocyte differentiation, we isolated stromal-vascular fraction (SVF) from BAT and studied the differentiation into thermogenic adipocytes. This model was chosen to more closely mimic the *in vivo* situation since the SVF contains both adipocyte precursors and endothelial cells. It is, however, important to note that these heterogeneous cell types may not be present throughout the time course of differentiation. Nevertheless, it has been shown that the endothelial compartment can give rise to adipogenic precursors that can differentiate into thermogenic adipocytes. The SVF model thus most likely represents a mix of cell-autonomous effects and cellular cross-talk. Treatment with TRL, but not with LDL (Figure S6I), throughout the differentiation resulted in higher expression of the thermogenic adipocyte markers *Pparg*, *Ppargc1a*, *Ucp1*, and *Dio2* (Figure 6M). Of note, the TRL-mediated induction of differentiation markers was completely blocked by LAL inhibition (Figure 6M), by the HIF1α inhibitor (Figure 6N), and by MitoQ treatment (Figure 6O). Taken together, these findings describe a direct role of

Figure 4. Endothelial LAL deletion causes impaired adaptive thermogenesis

Transgenic mice were treated with tamoxifen to generate mice lacking LAL in endothelial cells (*Lipa*$^{fl/fl}$-Cdh5^{Cre+}) and controls (*Lipa*$^{fl/fl}$-Cdh5^{Cre-}) and fed with a cholesterol-rich high-fat diet.

(A–F) shows mice acclimated to thermoneutrality (30°C) for 2 weeks, followed by 3 days at 18°C and 4 days at 6°C. (G–M) shows mice housed at room temperature, followed by 4-weeks chronic acclimation to 6°C.

(A) Energy expenditure. Body weights were 26.5 ± 1.1 g for *Lipa*$^{fl/fl}$-Cdh5^{Cre}-and 26.6 ± 0.5 g for *Lipa*$^{fl/fl}$-Cdh5^{Cre+} (n = 4).

(B) Quantification of day/night and diurnal energy expenditure, as shown in (A).

(C) Whole BAT uptake of ^{3}H-deoxyglucose (^{3}H-DOG) and ^{14}C-triolein-TRL after a combined oral glucose and fat gavage (n = 7–8).

(D) BAT gene expression (n = 7–8).

(E) Western blot of BAT including Ponceau staining.

(F) Quantification per BAT depot and normalization of UCP1 shown in (E) (n = 7).

(G) Energy expenditure. Body weights were 29.5 ± 0.9 g for *Lipa*$^{fl/fl}$-Cdh5^{Cre-} and 27.6 ± 0.9 g for *Lipa*$^{fl/fl}$-Cdh5^{Cre+} (n = 8).

(H) Quantification of day/night and diurnal energy expenditure, as shown in (G).

(I) Whole inguinal WAT (iWAT) uptake of ^{3}H-DOG and ^{14}C-triolein after a combined oral glucose and fat gavage (n = 4–9).

(J) Representative images of HE-stained iWAT. Scale bar, 50 μm.

(K) Gene expression in iWAT (n = 5–6).

(L) Western blot of iWAT including Ponceau staining.

(M) Quantification per iWAT depot and normalization of proteins shown in (L) (n = 5).

Data are presented as mean values ± SEM, $^{*}p < 0.05$ by Student's t test, *Lipa*$^{fl/fl}$-Cdh5^{Cre+} versus *Lipa*$^{fl/fl}$-Cdh5^{Cre-}. See also Figure S4.

Please cite this article in press as: Fischer et al., Lysosomal lipoprotein processing in endothelial cells stimulates adipose tissue thermogenic adaptation, Cell Metabolism (2020), https://doi.org/10.1016/j.cmet.2020.12.001

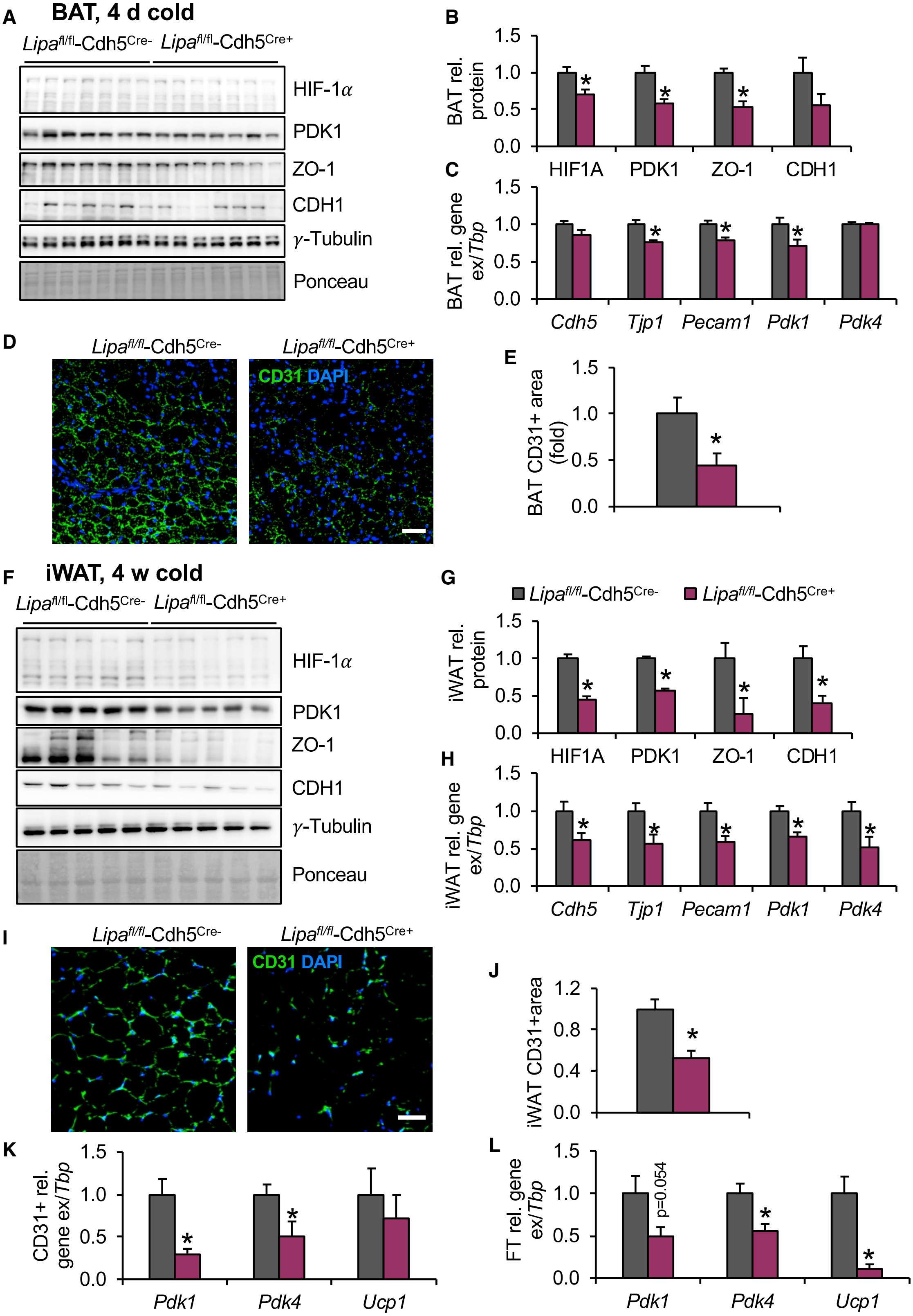

(legend on next page)

Please cite this article in press as: Fischer et al., Lysosomal lipoprotein processing in endothelial cells stimulates adipose tissue thermogenic adaptation, Cell Metabolism (2020), https://doi.org/10.1016/j.cmet.2020.12.001

lysosomal TRL processing in inducing proliferative responses via a mechanism involving fatty acid oxidation, ROS production and HIF1α induction in endothelial cells, and stromal-vascular cells from adipose tissue, ultimately promoting the differentiation of precursor cells into thermogenic adipocytes.

Discussion

The rediscovery of active thermogenic adipose tissues in adult humans has prompted a plethora of studies investigating the origin of thermogenic cells (Chouchani et al., 2019; Ikeda et al., 2018) and assessing the metabolic benefits of adaptive thermogenesis (Chen et al., 2020; Scheele and Wolfrum, 2020). Recently, it was demonstrated in a large retrospective study that the presence of active BAT inversely associates with cardiovascular disease and with its risk factor triglycerides (Becher et al., 2020). This observation confirms data generated in rodent models showing pronounced triglyceride-lowering and antiatherogenic effects mediated by active thermogenic adipose tissues (Bartelt et al., 2011; Berbée et al., 2015). These effects were linked to both accelerated intravascular LPL-mediated lipolysis of TRL and uptake of whole lipoprotein particles into activated BAT (Bartelt et al., 2011; Heine et al., 2018); yet, details of cellular trafficking and the physiological significance of TRL uptake remained elusive. In this study, we show that endothelial cells of thermogenic adipose tissues are the main cell type responsible for whole-TRL-particle uptake. Furthermore, we find that lysosomal TRL processing by LAL in endothelial cells is critical for efficient adaptive thermogenesis both in BAT and WAT.

By employing nanoparticle-based imaging techniques and tracer studies combined with cell sorting, we demonstrate that TRL remnants generated by LPL-dependent triglyceride hydrolysis are taken up by endocytosis into vascular endothelial cells. LPL is mandatory in this two-step process, presumably because the enzyme mediates the shrinkage of TRL to reach the upper size limit for particle endocytosis of nonphagocytic cells, which is approximately 100–200 nm (Rejman et al., 2004). Supporting this notion, administration of the pharmacological LPL-inhibitor tetrahydrolipstatin (Bartelt et al., 2011) or transgenic expression of the endogenous LPL-inhibitory protein angiopoietin-like 4 (Angptl4) (Dijk et al., 2015) diminishes LPL activity and subsequent TRL core-label uptake into thermogenic adipose tissues. The second step, the endocytosis of remnant particles, is dependent on CD36, which we found markedly induced in its abundance at the luminal side of the endothelium in BAT of mice exposed to cold. Global deletion of CD36 strongly attenuated the cold-induced whole-TRL-particle uptake into BAT. At the same time, the internalization was unaffected by CD36 deficiency in mice housed under warm ambient temperatures, pointing toward a role of other lipoprotein receptors for basal endocytosis into BAT. Recently, another example of endothelial lipoprotein particle uptake was reported in a pathophysiological context. In that elegant study, it was demonstrated that LDL particles undergo endothelial transcytosis via the scavenger receptor SR-B1, and thereby this process causes arterial cholesterol deposition and thus atherosclerosis (Huang et al., 2019). It is clear from our results that SR-B1 cannot compensate for the lack of CD36, arguing against an important role SR-B1 for TRL uptake and transcytosis in adipose tissues. In addition to the likely differences between arterial and capillary endothelium, another main difference between these studies is the lipoprotein particle composition and size. In the future it will be important to unravel the relevance of endothelial lipoprotein processing in other metabolically active organs, especially in the context of physiological adaptations and disease development, and it will be intriguing to compare the endocytic machinery of endothelial cells with that of other cell types such as hepatocytes (Gilleron et al., 2019).

Based on a single-cell transcriptome atlas of eleven organs not including adipose tissues, a specific subclass of lipid-handling endothelial cells in heart and skeletal muscles was recently identified. These specific endothelial cells were characterized by the expression of lipid and lipoprotein-processing genes including *Cd36 and Lpl* (Kalucka et al., 2020). Interestingly, a higher expression of CD36 and LPL in thermogenic adipose tissue of cold-exposed humans has been reported (Chondronikola et al., 2016), although the cellular origin of expression was not assessed in that study. Here, we show that in addition to *Cd36 and Lpl*, endothelial cells of thermogenic adipose tissues express *Lipa*, indicating that endothelial cells of thermogenic adipose tissue are equipped to metabolize internalized lipoproteins. LAL is the only lysosomal triglyceride and cholesterol ester hydrolase, and consequently, LAL deficiency in humans leads to the development of Wolman's disease, a lysosomal storage disorder, which is characterized by ectopic lipid accumulation especially in liver and spleen, atherosclerosis,

Figure 5. LAL modulates abundance of HIF1α and endothelial markers upon thermogenic recruitment

Lipa$^{fl/fl}$-Cdh5^{Cre+} and *Lipa*$^{fl/fl}$-Cdh5^{Cre-} mice were fed a cholesterol-rich high-fat diet.

(A–E) shows mice acclimated to 30°C for 2 weeks, followed by 3 days at 18°C and 4 days at 6°C. (F–L) shows mice housed at room temperature, followed by 4 weeks of chronic acclimation to 6°C.

(A) Western blot of BAT including Ponceau staining.

(B) Quantification of proteins shown in (A) (n = 7).

(C) BAT expression of endothelial marker genes and *Pdk1/4* (n = 7–8).

(D) Representative images of CD31 staining in BAT. Green=CD31, blue=DAPI, scale bar: 50 μm.

(E) Quantification of CD31 area in BAT sections as detected in (D) (n = 7–8).

(F) Western blot of iWAT including Ponceau staining.

(G) Quantification of proteins shown in (F) (n = 5).

(H) Expression of endothelial marker genes and *Pdk1/4* in iWAT (n = 6–8).

(I) Representative images of CD31 staining in iWAT. Green, CD31; blue, DAPI, scale bar, 50 μm.

(J) Quantification of CD31 area in iWAT as detected in (I) (n = 4).

(K) Gene expression in CD31$^+$ endothelial cells MACS®-isolated from iWAT (n = 3).

(L) Gene expression in adipocyte-enriched FT after MACS® of iWAT (n = 3).

Data are presented as mean values ± SEM, $^*p < 0.05$ by Student's t test comparing *Lipa*$^{fl/fl}$-Cdh5^{Cre+} versus *Lipa*$^{fl/fl}$-Cdh5^{Cre-}. See also Figure S5.

Please cite this article in press as: Fischer et al., Lysosomal lipoprotein processing in endothelial cells stimulates adipose tissue thermogenic adaptation, Cell Metabolism (2020), https://doi.org/10.1016/j.cmet.2020.12.001

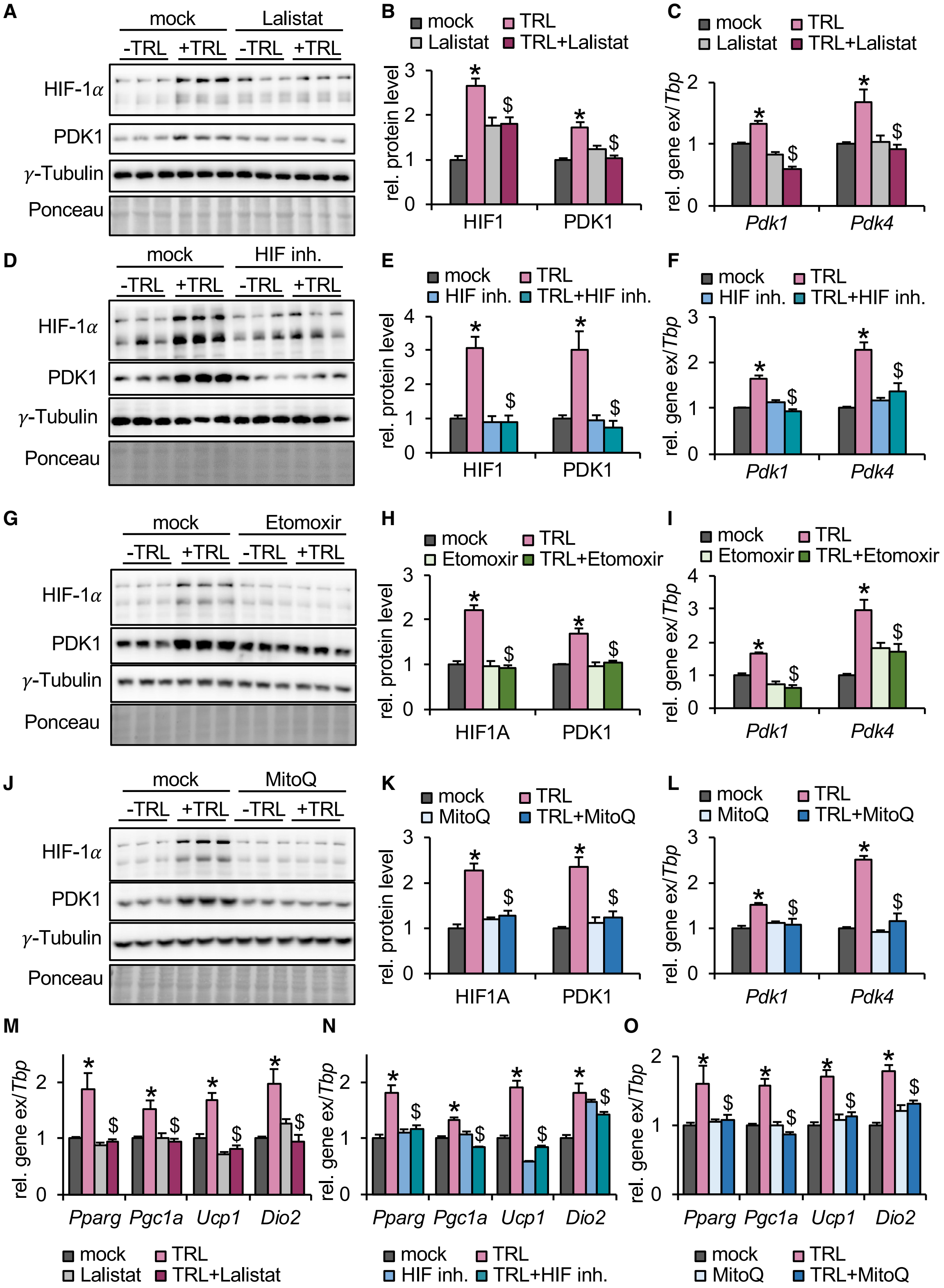

Figure 6. LAL-dependent TRL processing stimulates proliferation and thermogenic differentiation via HIF1α

Immortalized brown adipocyte precursor cells (WT1) and primary BAT stromal-vascular cells (SVC) were cultured in the absence (mock) or presence of lipoproteins (TRL). LAL was inhibited by Lalistat, HIF1α by a specific inhibitor, beta-oxidation by etomoxir, and mitochondrial ROS was scavenged MitoQ. Representative images are shown of two (G and J) or three (A and D) independent western blot experiments.

(legend continued on next page)

diarrhea, as well as pulmonary and neurological defects due to accumulation of cholesterol esters (Bernstein et al., 2013; Krivit et al., 1992). However, the relevance of LAL in endothelial cells has not been addressed so far. Here, we show that specific depletion of endothelial LAL causes impaired TRL processing, an alteration compromising the adaptation of thermogenic adipose tissues to a cold environment and thus thermogenesis. Under conditions of acute cold with previous acclimation to thermoneutrality, LAL deficiency blunted the thermogenic response in BAT but not in WAT. On the other hand, sustained cold exposure of mice had only subtle effects on classical BAT depots while pronounced differences in the number and function of brite/beige adipocytes in WAT were observed. Specific effects on thermogenic WAT remodeling with minor effects on BAT have been observed previously in other models. For example, inhibition of the sterol synthesis pathway by statins leads to impaired inguinal WAT browning with negligible effects on BAT thermogenic capacity (Balaz et al., 2019). The temporal difference observed in this study between BAT and WAT recruitment may be explained by distinct precursor populations responsible for the thermogenic recruitment, as well as in a higher proportion of already existing terminally differentiated thermogenic adipocytes in BAT compared with those in WAT (Kalinovich et al., 2017).

For optimal thermogenic function, adipose tissues require adequate vascularization to ensure sufficient supply of nutrients and oxygen, as well as to achieve rapid heat dissipation (Bagchi et al., 2013; Luo et al., 2017; Xue et al., 2009). Chronic cold exposure increases proliferation of endothelial cells and thus angiogenesis in both BAT and in inguinal WAT (Xue et al., 2009). We observed reduced levels of endothelial cell markers in inguinal WAT of cold-acclimated mice lacking LAL in endothelial cells. This indicates disturbed angiogenesis, a pathway that is mainly controlled by HIF1α (Corvera and Gealekman, 2014; Hirota and Semenza, 2006; Semenza and Wang, 1992). Notably, our data indicate that LAL-dependent TRL processing activates a HIF1α-dependent proliferative response of endothelial cells and is required for efficient differentiation of thermogenic precursors and browning. It has been shown that during the developmental phase angiogenesis precedes the appearance of adipocytes (Han et al., 2011). Importantly, various precursor cells including subsets with an endothelial origin that can differentiate to thermogenic adipocytes, have been described to reside in the vascular niche (Gupta et al., 2012; Min et al., 2016; Tang et al., 2008; Tran et al., 2012), thus directly linking the endothelium to the development of thermogenic BAT and WAT. We observed stimulating effects of TRL on adipogenesis in the SVF, which next to endothelial cells also contains various adipocyte precursors (Vishvanath and Gupta, 2019). Future studies are warranted to investigate whether TRL stimulate browning primarily by angiogenesis or by paracrine factors released from endothelial cells that promote thermogenic precursor differentiation. Importantly, the positive effect on adipocyte differentiation was only observed for TRL but not for LDL, which argues against a role for cholesterol and derivatives thereof that may influence thermogenic adipocyte formation. It is also increasingly recognized that fatty acid metabolism in endothelial cells is a key determinant of angiogenesis (Li et al., 2019a). In support of this hypothesis, here, we show that inhibition of beta-oxidation and ROS production can effectively block the proliferative and differentiative effects of TRLs, arguing for a role of fatty acid catabolism in this process. Additionally, there are a number of lipids transported by TRL that are released by LAL and could affect thermogenic differentiation. For instance, the bioactive derivative of vitamin A, retinoic acid, has been described to stimulate the VEGF-dependent brite/beige adipocyte differentiation from endothelial niche precursors (Wang et al., 2017). TRL particles contain retinol esters that can be converted into retinoic acid in adipose tissues (Kiefer et al., 2012; Krois et al., 2019), and our data show that radiolabeled retinol incorporated into TRL is readily taken up by endothelial cells. In addition, PUFAs as well as their derivative prostaglandins have been shown to induce adipose tissue browning (Ghandour et al., 2018; Vegiopoulos et al., 2010), and to affect—at least in the context of the tumor microenvironment—HIF1α activity (Krishnamoorthy and Honn, 2011). It is important to note that, in addition to the effects of fatty acid catabolism and subsequent HIF1α activity, fatty acids liberated by LAL could also affect the activity of ligand-activated transcription factors regulating thermogenic gene expression, such as PPARγ. Thus, next to the effects of endothelial TRL processing on HIF1α activity described in this study, other fatty-acid-dependent mechanisms may contribute to the TRL-dependent thermogenic differentiation pathway.

Taken together, this study shows that internalization and processing of lipoproteins in capillary endothelial cells determines thermogenic function and browning of adipose tissues. Future studies based on this novel aspect of adaptive thermogenesis are warranted to identify TRL responsive endothelial and/or

(A) Effect of TRL and Lalistat on HIF1α and PDK1 protein levels in WT1 cells.
(B) Quantification of proteins described in (A) (n = 9).
(C) Effect of TRL and Lalistat on *Pdk1* and *Pdk4* expression in WT1 cells (n = 9).
(D) Effect of TRL and HIF1α inhibitor on HIF1α and PDK1 protein levels in WT1 cells.
(E) Quantification of proteins described in (D) (n = 9).
(F) Effect of TRL and HIF1α inhibitor on *Pdk1* and *Pdk4* expression in WT1 cells (n = 9).
(G) Effect of TRL and etomoxir on HIF1α and PDK1 protein levels in WT1 cells.
(H) Quantification of proteins described in (G) (n = 6).
(I) Effect of TRL and etomoxir on *Pdk1* and *Pdk4* expression in WT1 cells (n = 6).
(J) Effect of TRL and MitoQ on HIF1α and PDK1 protein levels in WT1 cells.
(K) Quantification of proteins described in (J) (n = 6).
(L) Effect of TRL and MitoQ on *Pdk1* and *Pdk4* expression in WT1 cells (n = 6).
(M) Thermogenic gene expression of SVC differentiated for 7 days with or without TRL ± Lalistat (n = 7).
(N) Thermogenic gene expression of SVC differentiated for 7 days with or without TRL ± HIF1α inhibitor (n = 6).
(O) Thermogenic gene expression of SVC differentiated for 7 days with or without TRL ± MitoQ (n = 8).
Data are presented as mean values ± SEM. $p < 0.05$ by ANOVA comparing mock versus TRL(*) and TRL versus TRL + inhibitors ($). See also Figure S6.

Please cite this article in press as: Fischer et al., Lysosomal lipoprotein processing in endothelial cells stimulates adipose tissue thermogenic adaptation, Cell Metabolism (2020), https://doi.org/10.1016/j.cmet.2020.12.001

adipocyte precursor subtypes. In addition, single-cell transcriptomics with samples from cold-exposed mice and humans would be a promising approach to investigate the roles of endothelial subtypes expressing lipoprotein-processing enzymes, including LAL, in thermogenic adipose tissues.

Limitations of study

In this study, we show a role of endothelial LAL for the recruitment of thermogenic adipose tissues. We chose a tamoxifen-inducible, endothelial-cell-specific Cre system to exclude potential undesired effects of *Lipa* depletion in nonendothelial cells during embryonic development. However, this may have masked relevant effects of LAL during early development. In this context, it is of note that there is no Cre system specific to the endothelial cells of adipose tissues. Therefore, effects on endothelial cells in other organs, e.g., the heart, even though not readily visible in our studies, may contribute to some of our findings, such as reduced body-core temperature in the cold. In humans, the overall importance of LAL is easily seen by the drastic phenotype of Wolman's disease (Li and Zhang, 2019), which, however, is probably mostly related to LAL function in hepatocytes. Thus, establishing a role of endothelial cell LAL in humans will prove more difficult but may be overcome by the use of single-cell sequencing of biopsied BAT after controlled cold-intervention studies. Another important factor to note is that our *in vitro* settings of preadipocytes and endothelial cells do not recapitulate the complex cellular interactions that are most likely taking place *in vivo*. We show that TRL can affect endothelial cell and adipocyte precursor proliferation and differentiation in a LAL and HIF1α-dependent manner. However, these experiments do not address conceivable effects of paracrine factors released by endothelial cells in response to intracellular TRL processing. Future studies are necessary to identify the nature of these potential molecular mediators and to explore the proposed endothelial cell-adipocyte cross-talk.

STAR★methods

Detailed methods are provided in the online version of this paper and include the following:

- KEY RESOURCES TABLE
- RESOURCE AVAILABILITY
    - ○ Lead contact
    - ○ Materials availability
    - ○ Data and code availability
- EXPERIMENTAL MODEL AND SUBJECT DETAILS
    - ○ Mice
    - ○ Clinical Studies
- METHOD DETAILS
    - ○ Preparation of TRL
    - ○ Metabolic turnover studies
    - ○ Isolation of endothelial cells, tissue-resident macrophages and brown adipocytes
    - ○ Immunofluorescence, transmission electron microscopy and HE-staining
    - ○ Intravital microscopy and magnetic resonance imaging
    - ○ *In vivo* biotinylation
    - ○ Magnetic organelle isolation
    - ○ Cell culture
    - ○ Western blotting
    - ○ Indirect calorimetry
    - ○ Measurement of heat-loss and body temperature
    - ○ Gene expression Analysis of murine samples
    - ○ RNAseq of human BAT samples
    - ○ Lipidomic analysis using MS/MS approach
- QUANTIFICATION AND STATISTICAL ANALYSIS

Supplemental information

Supplemental Information can be found online at https://doi.org/10.1016/j.cmet.2020.12.001.

Acknowledgments

A.W.F. was supported by the German National Academic Foundation, DFG (Fi2476/1-1) and HFSP (LT000936/2020) and by DACH Gesellschaft für Lipidologie. L.S. was supported by DFG grant SCHE522/4-1. J.H. was supported by DFG grants HE3645/10-1, project-ID:335447727-SFB1328 and by BMBF 13XP5079C. K.G. was supported by a fellowship from the Schering foundation. L.S. and M.H. were supported by the Mühlbauer Stiftung. C.S. was supported by a fellowship from Gertraud und Heinz Rose Stiftung and the UKE MD/PhD program fellowship. O.C. was supported by a Brown University startup fund. The authors thank Sandra Ehret and Birgit Henkel for technical assistance. We thank Tobias Walther and Robert Farese, Jr. for fruitful discussions.

Author contributions

A.W.F., M.Y.J., L.S., and J.H. designed the study. A.W.F., L.S., and J.H. wrote the manuscript. A.W.F., M.Y.J., K.G., M.H., F.S., N.M., C.S., A.W., O.T.B., H.I., S.K.N., P.S., J.U., M.B., H.D., R.R., and W.S. researched data. Y.Y., H.Z., and O.C. generated QDs. All authors contributed to data discussion and approved the final manuscript.

Declaration of interests

The authors declare no competing interests.

Received: May 19, 2020
Revised: October 2, 2020
Accepted: November 30, 2020
Published: December 22, 2020

References

Aran, D., Looney, A.P., Liu, L., Wu, E., Fong, V., Hsu, A., Chak, S., Naikawadi, R.P., Wolters, P.J., Abate, A.R., et al. (2019). Reference-based analysis of lung single-cell sequencing reveals a transitional profibrotic macrophage. Nat. Immunol. *20*, 163–172.

Asano, A., Morimatsu, M., Nikami, H., Yoshida, T., and Saito, M. (1997). Adrenergic activation of vascular endothelial growth factor mRNA expression in rat brown adipose tissue: implication in cold-induced angiogenesis. Biochem. J. *328*, 179–183.

Bagchi, M., Kim, L.A., Boucher, J., Walshe, T.E., Kahn, C.R., and D'Amore, P.A. (2013). Vascular endothelial growth factor is important for brown adipose tissue development and maintenance. FASEB J. *27*, 3257–3271.

Balaz, M., Becker, A.S., Balazova, L., Straub, L., Müller, J., Gashi, G., Maushart, C.I., Sun, W., Dong, H., Moser, C., et al. (2019). Inhibition of mevalonate pathway prevents adipocyte browning in mice and men by affecting protein prenylation. Cell Metab. *29*, 901–916.e8.

Bartelt, A., Bruns, O.T., Reimer, R., Hohenberg, H., Ittrich, H., Peldschus, K., Kaul, M.G., Tromsdorf, U.I., Weller, H., Waurisch, C., et al. (2011). Brown adipose tissue activity controls triglyceride clearance. Nat. Med. *17*, 200–205.

Bartelt, A., and Heeren, J. (2014). Adipose tissue browning and metabolic health. Nat. Rev. Endocrinol. *10*, 24–36.

Please cite this article in press as: Fischer et al., Lysosomal lipoprotein processing in endothelial cells stimulates adipose tissue thermogenic adaptation, Cell Metabolism (2020), https://doi.org/10.1016/j.cmet.2020.12.001

Bartelt, A., John, C., Schaltenberg, N., Berbée, J.F.P., Worthmann, A., Cherradi, M.L., Schlein, C., Piepenburg, J., Boon, M.R., Rinninger, F., et al. (2017). Thermogenic adipocytes promote HDL turnover and reverse cholesterol transport. Nat. Commun. *8*, 15010.

Becher, T., Palanisamy, S., Kramer, D.J., Marx, S.J., Wibmer, A.G., Del Gaudio, I., Butler, S.D., Jiang, C.S., Vaughan, R., Schöder, H., et al. (2020). Brown adipose tissue is associated with improved cardiometabolic health and regulates blood pressure. bioRxiv. https://doi.org/10.1101/2020.02.08.933754v1.

Beigneux, A.P., Davies, B.S., Gin, P., Weinstein, M.M., Farber, E., Qiao, X., Peale, F., Bunting, S., Walzem, R.L., Wong, J.S., et al. (2007). Glycosylphosphatidylinositol-anchored high-density lipoprotein-binding protein 1 plays a critical role in the lipolytic processing of chylomicrons. Cell Metab. *5*, 279–291.

Beigneux, A.P., Franssen, R., Bensadoun, A., Gin, P., Melford, K., Peter, J., Walzem, R.L., Weinstein, M.M., Davies, B.S., Kuivenhoven, J.A., et al. (2009). Chylomicronemia with a mutant GPIHBP1 (Q115P) that cannot bind lipoprotein lipase. Arterioscler. Thromb. Vasc. Biol. *29*, 956–962.

Berbée, J.F., Boon, M.R., Khedoe, P.P., Bartelt, A., Schlein, C., Worthmann, A., Kooijman, S., Hoeke, G., Mol, I.M., John, C., et al. (2015). Brown fat activation reduces hypercholesterolaemia and protects from atherosclerosis development. Nat. Commun. *6*, 6356.

Bernstein, D.L., Hülkova, H., Bialer, M.G., and Desnick, R.J. (2013). Cholesteryl ester storage disease: review of the findings in 135 reported patients with an underdiagnosed disease. J. Hepatol. *58*, 1230–1243.

Bruns, O.T., Bischof, T.S., Harris, D.K., Franke, D., Shi, Y., Riedemann, L., Bartelt, A., Jaworski, F.B., Carr, J.A., Rowlands, C.J., et al. (2017). Next-generation in vivo optical imaging with short-wave infrared quantum dots. Nat. Biomed. Eng. *1*, 0056.

Bruns, O.T., Ittrich, H., Peldschus, K., Kaul, M.G., Tromsdorf, U.I., Lauterwasser, J., Nikolic, M.S., Mollwitz, B., Merkel, M., Bigall, N.C., et al. (2009). Real-time magnetic resonance imaging and quantification of lipoprotein metabolism in vivo using nanocrystals. Nat. Nanotechnol. *4*, 193–201.

Cannon, B., and Nedergaard, J. (2004). Brown adipose tissue: function and physiological significance. Physiol. Rev. *84*, 277–359.

Cao, Y. (2009). Positive and negative modulation of angiogenesis by VEGFR1 ligands. Sci Signal. *2*, re1.

Chen, K.Y., Brychta, R.J., Abdul Sater, Z., Cassimatis, T.M., Cero, C., Fletcher, L.A., Israni, N.S., Johnson, J.W., Lea, H.J., Linderman, J.D., et al. (2020). Opportunities and challenges in the therapeutic activation of human energy expenditure and thermogenesis to manage obesity. J. Biol. Chem. *295*, 1926–1942.

Chen, O., Zhao, J., Chauhan, V.P., Cui, J., Wong, C., Harris, D.K., Wei, H., Han, H.S., Fukumura, D., Jain, R.K., and Bawendi, M.G. (2013). Compact high-quality CdSe-CdS core-shell nanocrystals with narrow emission linewidths and suppressed blinking. Nat. Mater. *12*, 445–451.

Chondronikola, M., Volpi, E., Børsheim, E., Porter, C., Saraf, M.K., Annamalai, P., Yfanti, C., Chao, T., Wong, D., Shinoda, K., et al. (2016). Brown adipose tissue activation is linked to distinct systemic effects on lipid metabolism in humans. Cell Metab. *23*, 1200–1206.

Chouchani, E.T., Kazak, L., and Spiegelman, B.M. (2019). New advances in adaptive thermogenesis: UCP1 and beyond. Cell Metab. *29*, 27–37.

Corvera, S., and Gealekman, O. (2014). Adipose tissue angiogenesis: impact on obesity and type-2 diabetes. Biochim Biophys Acta *1842*, 463–472.

Dickinson, M.E., Flenniken, A.M., Ji, X., Teboul, L., Wong, M.D., White, J.K., Meehan, T.F., Weninger, W.J., Westerberg, H., Adissu, H., et al. (2016). High-throughput discovery of novel developmental phenotypes. Nature *537*, 508–514.

Dijk, W., Heine, M., Vergnes, L., Boon, M.R., Schaart, G., Hesselink, M.K., Reue, K., van Marken Lichtenbelt, W.D., Olivecrona, G., Rensen, P.C., et al. (2015). ANGPTL4 mediates shuttling of lipid fuel to brown adipose tissue during sustained cold exposure. eLife *4*, e08428.

Du, H., Heur, M., Duanmu, M., Grabowski, G.A., Hui, D.Y., Witte, D.P., and Mishra, J. (2001). Lysosomal acid lipase-deficient mice: depletion of white and brown fat, severe hepatosplenomegaly, and shortened life span. J. Lipid Res. *42*, 489–500.

Duta-Mare, M., Sachdev, V., Leopold, C., Kolb, D., Vujic, N., Korbelius, M., Hofer, D.C., Xia, W., Huber, K., Auer, M., et al. (2018). Lysosomal acid lipase regulates fatty acid channeling in brown adipose tissue to maintain thermogenesis. Biochim Biophys Acta Mol Cell Biol Lipids *1863*, 467–478.

Elias, I., Franckhauser, S., Ferré, T., Vilà, L., Tafuro, S., Muñoz, S., Roca, C., Ramos, D., Pujol, A., Riu, E., et al. (2012). Adipose tissue overexpression of vascular endothelial growth factor protects against diet-induced obesity and insulin resistance. Diabetes *61*, 1801–1813.

Fischer, A.W., Albers, K., Krott, L.M., Hoffzimmer, B., Heine, M., Schmale, H., Scheja, L., Gordts, P.L.S.M., and Heeren, J. (2018a). The adaptor protein PID1 regulates receptor-dependent endocytosis of postprandial triglyceride-rich lipoproteins. Mol. Metab. *16*, 88–99.

Fischer, A.W., Cannon, B., and Nedergaard, J. (2018b). Optimal housing temperatures for mice to mimic the thermal environment of humans: an experimental study. Mol. Metab. *7*, 161–170.

Fischer, A.W., Hoefig, C.S., Abreu-Vieira, G., de Jong, J.M.A., Petrovic, N., Mittag, J., Cannon, B., and Nedergaard, J. (2016). Leptin raises defended body temperature without activating thermogenesis. Cell Rep. *14*, 1621–1631.

Fischer, A.W., Schlein, C., Cannon, B., Heeren, J., and Nedergaard, J. (2019). Intact innervation is essential for diet-induced recruitment of brown adipose tissue. Am. J. Physiol. Endocrinol. Metab. *316*, E487–E503.

Fischer, A.W., Shabalina, I.G., Mattsson, C.L., Abreu-Vieira, G., Cannon, B., Nedergaard, J., and Petrovic, N. (2017). UCP1 inhibition in Cidea-overexpressing mice is physiologically counteracted by brown adipose tissue hyperrecruitment. Am. J. Physiol. Endocrinol. Metab. *312*, E72–E87.

Fredriksson, J.M., Nikami, H., and Nedergaard, J. (2005). Cold-induced expression of the VEGF gene in brown adipose tissue is independent of thermogenic oxygen consumption. FEBS Lett. *579*, 5680–5684.

Furler, S.M., Cooney, G.J., Hegarty, B.D., Lim-Fraser, M.Y., Kraegen, E.W., and Oakes, N.D. (2000). Local factors modulate tissue-specific NEFA utilization: assessment in rats using 3H-(R)-2-bromopalmitate. Diabetes *49*, 1427–1433.

Gealekman, O., Burkart, A., Chouinard, M., Nicoloro, S.M., Straubhaar, J., and Corvera, S. (2008). Enhanced angiogenesis in obesity and in response to PPARgamma activators through adipocyte VEGF and ANGPTL4 production. Am. J. Physiol. Endocrinol. Metab. *295*, E1056–E1064.

Ghandour, R.A., Colson, C., Giroud, M., Maurer, S., Rekima, S., Ailhaud, G., Klingenspor, M., Amri, E.Z., and Pisani, D.F. (2018). Impact of dietary ω3 polyunsaturated fatty acid supplementation on brown and Brite adipocyte function. J. Lipid Res. *59*, 452–461.

Gilleron, J., Gerdes, J.M., and Zeigerer, A. (2019). Metabolic regulation through the endosomal system. Traffic *20*, 552–570.

Goldberg, I.J., Eckel, R.H., and Abumrad, N.A. (2009). Regulation of fatty acid uptake into tissues: lipoprotein lipase- and CD36-mediated pathways. J. Lipid Res. *50*, S86–S90.

Gupta, R.K., Mepani, R.J., Kleiner, S., Lo, J.C., Khandekar, M.J., Cohen, P., Frontini, A., Bhowmick, D.C., Ye, L., Cinti, S., and Spiegelman, B.M. (2012). Zfp423 expression identifies committed preadipocytes and localizes to adipose endothelial and perivascular cells. Cell Metab. *15*, 230–239.

Han, J., Lee, J.E., Jin, J., Lim, J.S., Oh, N., Kim, K., Chang, S.I., Shibuya, M., Kim, H., and Koh, G.Y. (2011). The spatiotemporal development of adipose tissue. Development *138*, 5027–5037.

Heine, M., Fischer, A.W., Schlein, C., Jung, C., Straub, L.G., Gottschling, K., Mangels, N., Yuan, Y., Nilsson, S.K., Liebscher, G., et al. (2018). Lipolysis triggers a systemic insulin response essential for efficient energy replenishment of activated brown adipose tissue in mice. Cell Metab *28*, 644–655.e4.

Hirota, K., and Semenza, G.L. (2006). Regulation of angiogenesis by hypoxia-inducible factor 1. Crit. Rev. Oncol. Hematol. *59*, 15–26.

Huang, L., Chambliss, K.L., Gao, X., Yuhanna, I.S., Behling-Kelly, E., Bergaya, S., Ahmed, M., Michaely, P., Luby-Phelps, K., Darehshouri, A., et al. (2019). SR-B1 drives endothelial cell LDL transcytosis via DOCK4 to promote atherosclerosis. Nature *569*, 565–569.

Hultin, M., Savonen, R., and Olivecrona, T. (1996). Chylomicron metabolism in rats: lipolysis, recirculation of triglyceride-derived fatty acids in plasma FFA, and fate of core lipids as analyzed by compartmental modelling. J. Lipid Res. *37*, 1022–1036.

Ikeda, K., Maretich, P., and Kajimura, S. (2018). The common and distinct features of brown and beige adipocytes. Trends Endocrinol. Metab. *29*, 191–200.

Jung, S.N., Yang, W.K., Kim, J., Kim, H.S., Kim, E.J., Yun, H., Park, H., Kim, S.S., Choe, W., Kang, I., and Ha, J. (2008). Reactive oxygen species stabilize hypoxia-inducible factor-1 alpha protein and stimulate transcriptional activity via AMP-activated protein kinase in DU145 human prostate cancer cells. Carcinogenesis *29*, 713–721.

Kalinovich, A.V., de Jong, J.M., Cannon, B., and Nedergaard, J. (2017). UCP1 in adipose tissues: two steps to full browning. Biochimie *134*, 127–137.

Kalucka, J., de Rooij, L.P.M.H., Goveia, J., Rohlenova, K., Dumas, S.J., Meta, E., Conchinha, N.V., Taverna, F., Teuwen, L.A., Veys, K., et al. (2020). Single-cell transcriptome atlas of murine endothelial cells. Cell *180*, 764–779.e20.

Kiefer, F.W., Vernochet, C., O'Brien, P., Spoerl, S., Brown, J.D., Nallamshetty, S., Zeyda, M., Stulnig, T.M., Cohen, D.E., Kahn, C.R., and Plutzky, J. (2012). Retinaldehyde dehydrogenase 1 regulates a thermogenic program in white adipose tissue. Nat. Med. *18*, 918–925.

Klein, J., Fasshauer, M., Ito, M., Lowell, B.B., Benito, M., and Kahn, C.R. (1999). beta(3)-adrenergic stimulation differentially inhibits insulin signaling and decreases insulin-induced glucose uptake in brown adipocytes. J. Biol. Chem. *274*, 34795–34802.

Krishnamoorthy, S., and Honn, K.V. (2011). Eicosanoids and other lipid mediators and the tumor hypoxic microenvironment. Cancer Metastasis Rev. *30*, 613–618.

Krivit, W., Freese, D., Chan, K.W., and Kulkarni, R. (1992). Wolman's disease: a review of treatment with bone marrow transplantation and considerations for the future. Bone Marrow Transplant *10*, 97–101.

Krois, C.R., Vuckovic, M.G., Huang, P., Zaversnik, C., Liu, C.S., Gibson, C.E., Wheeler, M.R., Obrochta, K.M., Min, J.H., Herber, C.B., et al. (2019). RDH1 suppresses adiposity by promoting brown adipose adaptation to fasting and re-feeding. Cell. Mol. Life Sci. *76*, 2425–2447.

Larsson, M., Allan, C.M., Heizer, P.J., Tu, Y., Sandoval, N.P., Jung, R.S., Walzem, R.L., Beigneux, A.P., Young, S.G., and Fong, L.G. (2018). Impaired thermogenesis and sharp increases in plasma triglyceride levels in GPIHBP1-deficient mice during cold exposure. J. Lipid Res. *59*, 706–713.

Li, F., and Zhang, H. (2019). Lysosomal acid lipase in lipid metabolism and beyond. Arterioscler. Thromb. Vasc. Biol. *39*, 850–856.

Li, X., Kumar, A., and Carmeliet, P. (2019a). Metabolic pathways fueling the endothelial cell drive. Annu. Rev. Physiol. *81*, 483–503.

Li, X., Sun, X., and Carmeliet, P. (2019b). Hallmarks of endothelial cell metabolism in health and disease. Cell Metab. *30*, 414–433.

Luo, X., Jia, R., Luo, X.Q., Wang, G., Zhang, Q.L., Qiao, H., Wang, N., and Yan, J.Q. (2017). Cold exposure differentially stimulates angiogenesis in BAT and WAT of mice: implication in adrenergic activation. Cell. Physiol. Biochem. *42*, 974–986.

Lynes, M.D., Leiria, L.O., Lundh, M., Bartelt, A., Shamsi, F., Huang, T.L., Takahashi, H., Hirshman, M.F., Schlein, C., Lee, A., et al. (2017). The cold-induced lipokine 12,13-diHOME promotes fatty acid transport into brown adipose tissue. Nat. Med. *23*, 631–637.

McGinnis, C.S., Murrow, L.M., and Gartner, Z.J. (2019). DoubletFinder: doublet detection in single-cell RNA sequencing data using artificial nearest neighbors. Cell Syst. *8*, 329–337.e4.

Min, S.Y., Kady, J., Nam, M., Rojas-Rodriguez, R., Berkenwald, A., Kim, J.H., Noh, H.L., Kim, J.K., Cooper, M.P., Fitzgibbons, T., et al. (2016). Human 'Brite/beige' adipocytes develop from capillary networks, and their implantation improves metabolic homeostasis in mice. Nat. Med. *22*, 312–318.

Monvoisin, A., Alva, J.A., Hofmann, J.J., Zovein, A.C., Lane, T.F., and Iruela-Arispe, M.L. (2006). VE-cadherin-CreERT2 transgenic mouse: a model for inducible recombination in the endothelium. Dev. Dyn. *235*, 3413–3422.

Movafagh, S., Crook, S., and Vo, K. (2015). Regulation of hypoxia-inducible factor-1a by reactive oxygen species: new developments in an old debate. J. Cell. Biochem. *116*, 696–703.

Ohno, H., Shinoda, K., Spiegelman, B.M., and Kajimura, S. (2012). PPARgamma agonists induce a white-to-brown fat conversion through stabilization of PRDM16 protein. Cell Metab. *15*, 395–404.

Park, J., Kim, M., Sun, K., An, Y.A., Gu, X., and Scherer, P.E. (2017). VEGF-A-expressing adipose tissue shows rapid beiging and enhanced survival After transplantation and confers IL-4-independent metabolic improvements. Diabetes *66*, 1479–1490.

Petrovic, N., Shabalina, I.G., Timmons, J.A., Cannon, B., and Nedergaard, J. (2008). Thermogenically competent nonadrenergic recruitment in brown preadipocytes by a PPARgamma agonist. Am. J. Physiol. Endocrinol. Metab. *295*, E287–E296.

Petrovic, N., Walden, T.B., Shabalina, I.G., Timmons, J.A., Cannon, B., and Nedergaard, J. (2010). Chronic peroxisome proliferator-activated receptor gamma (PPARgamma) activation of epididymally derived white adipocyte cultures reveals a population of thermogenically competent, UCP1-containing adipocytes molecularly distinct from classic brown adipocytes. J. Biol. Chem. *285*, 7153–7164.

Rejman, J., Oberle, V., Zuhorn, I.S., and Hoekstra, D. (2004). Size-dependent internalization of particles via the pathways of clathrin- and caveolae-mediated endocytosis. Biochem. J. *377*, 159–169.

Rosenbaum, A.I., Cosner, C.C., Mariani, C.J., Maxfield, F.R., Wiest, O., and Helquist, P. (2010). Thiadiazole carbamates: potent inhibitors of lysosomal acid lipase and potential Niemann-Pick type C disease therapeutics. J. Med. Chem. *53*, 5281–5289.

Rosenwald, M., Perdikari, A., Rülicke, T., and Wolfrum, C. (2013). Bi-directional interconversion of Brite and white adipocytes. Nat. Cell Biol. *15*, 659–667.

Scheele, C., and Wolfrum, C. (2020). Brown adipose crosstalk in tissue plasticity and human metabolism. Endocr. Rev. *41*, 53–65.

Scheja, L., and Heeren, J. (2016). Metabolic interplay between white, beige, brown adipocytes and the liver. J. Hepatol. *64*, 1176–1186.

Schlein, C., Talukdar, S., Heine, M., Fischer, A.W., Krott, L.M., Nilsson, S.K., Brenner, M.B., Heeren, J., and Scheja, L. (2016). FGF21 lowers plasma triglycerides by accelerating lipoprotein catabolism in white and brown adipose tissues. Cell Metab *23*, 441–453.

Seki, T., Hosaka, K., Lim, S., Fischer, C., Honek, J., Yang, Y., Andersson, P., Nakamura, M., Näslund, E., Ylä-Herttuala, S., et al. (2016). Endothelial PDGF-CC regulates angiogenesis-dependent thermogenesis in beige fat. Nat. Commun. *7*, 12152.

Semenza, G.L., and Wang, G.L. (1992). A nuclear factor induced by hypoxia via de novo protein synthesis binds to the human erythropoietin gene enhancer at a site required for transcriptional activation. Mol. Cell. Biol. *12*, 5447–5454.

Shabalina, I.G., Petrovic, N., de Jong, J.M., Kalinovich, A.V., Cannon, B., and Nedergaard, J. (2013). UCP1 in Brite/beige adipose tissue mitochondria is functionally thermogenic. Cell Rep. *5*, 1196–1203.

Son, N.H., Basu, D., Samovski, D., Pietka, T.A., Peche, V.S., Willecke, F., Fang, X., Yu, S.Q., Scerbo, D., Chang, H.R., et al. (2018). Endothelial cell CD36 optimizes tissue fatty acid uptake. J. Clin. Invest. *128*, 4329–4342.

Stanford, K.I., Middelbeek, R.J., Townsend, K.L., An, D., Nygaard, E.B., Hitchcox, K.M., Markan, K.R., Nakano, K., Hirshman, M.F., Tseng, Y.-H., and Goodyear, L.J. (2013). Brown adipose tissue regulates glucose homeostasis and insulin sensitivity. J. Clin. Invest. *123*, 215–223.

Stuart, T., Butler, A., Hoffman, P., Hafemeister, C., Papalexi, E., Mauck, W.M., 3rd, Hao, Y., Stoeckius, M., Smibert, P., and Satija, R. (2019). Comprehensive integration of single-cell data. Cell *177*, 1888–1902.e21.

Sun, K., Wernstedt Asterholm, I., Kusminski, C.M., Bueno, A.C., Wang, Z.V., Pollard, J.W., Brekken, R.A., and Scherer, P.E. (2012). Dichotomous effects of VEGF-A on adipose tissue dysfunction. Proc. Natl. Acad. Sci. USA *109*, 5874–5879.

Sun, W., Dong, H., Balaz, M., Slyper, M., Drokhlyansky, E., Colleluori, G., Giordano, A., Kovanicova, Z., Stefanicka, P., Balazova, L., et al. (2020).

snRNA-seq reveals a subpopulation of adipocytes that regulates thermogenesis. Nature *587*, 98–102.

Sung, H.K., Doh, K.O., Son, J.E., Park, J.G., Bae, Y., Choi, S., Nelson, S.M., Cowling, R., Nagy, K., Michael, I.P., et al. (2013). Adipose vascular endothelial growth factor regulates metabolic homeostasis through angiogenesis. Cell Metab. *17*, 61–72.

Tang, W., Zeve, D., Suh, J.M., Bosnakovski, D., Kyba, M., Hammer, R.E., Tallquist, M.D., and Graff, J.M. (2008). White fat progenitor cells reside in the adipose vasculature. Science *322*, 583–586.

Tran, K.V., Gealekman, O., Frontini, A., Zingaretti, M.C., Morroni, M., Giordano, A., Smorlesi, A., Perugini, J., De Matteis, R., Sbarbati, A., et al. (2012). The vascular endothelium of the adipose tissue gives rise to both white and brown fat cells. Cell Metab. *15*, 222–229.

Vegiopoulos, A., Müller-Decker, K., Strzoda, D., Schmitt, I., Chichelnitskiy, E., Ostertag, A., Berriel Diaz, M., Rozman, J., Hrabe de Angelis, M., Nüsing, R.M., et al. (2010). Cyclooxygenase-2 controls energy homeostasis in mice by de novo recruitment of brown adipocytes. Science *328*, 1158–1161.

Vishvanath, L., and Gupta, R.K. (2019). Contribution of adipogenesis to healthy adipose tissue expansion in obesity. J. Clin. Invest. *129*, 4022–4031.

Wang, B., Fu, X., Liang, X., Deavila, J.M., Wang, Z., Zhao, L., Tian, Q., Zhao, J., Gomez, N.A., Trombetta, S.C., et al. (2017). Retinoic acid induces white adipose tissue browning by increasing adipose vascularity and inducing beige adipogenesis of PDGFRα+ adipose progenitors. Cell Discov. *3*, 17036.

Wang, J., Qian, Y., and Gao, M. (2019). Overexpression of PDK4 is associated with cell proliferation, drug resistance and poor prognosis in ovarian cancer. Cancer Manag. Res. *11*, 251–262.

Wolock, S.L., Lopez, R., and Klein, A.M. (2019). Scrublet: computational identification of cell doublets in single-cell transcriptomic data. Cell Syst. *8*, 281–291.e9.

Woolbright, B.L., Choudhary, D., Mikhalyuk, A., Trammel, C., Shanmugam, S., Abbott, E., Pilbeam, C.C., and Taylor, J.A., 3rd. (2018). The role of pyruvate dehydrogenase kinase-4 (PDK4) in bladder cancer and chemoresistance. Mol. Cancer Ther. *17*, 2004–2012.

Worthmann, A., John, C., Rühlemann, M.C., Baguhl, M., Heinsen, F.A., Schaltenberg, N., Heine, M., Schlein, C., Evangelakos, I., Mineo, C., et al. (2017). Cold-induced conversion of cholesterol to bile acids in mice shapes the gut microbiome and promotes adaptive thermogenesis. Nat. Med. *23*, 839–849.

Wu, J., Boström, P., Sparks, L.M., Ye, L., Choi, J.H., Giang, A.H., Khandekar, M., Virtanen, K.A., Nuutila, P., Schaart, G., et al. (2012). Beige adipocytes are a distinct type of thermogenic fat cell in mouse and human. Cell *150*, 366–376.

Xue, Y., Petrovic, N., Cao, R., Larsson, O., Lim, S., Chen, S., Feldmann, H.M., Liang, Z., Zhu, Z., Nedergaard, J., et al. (2009). Hypoxia-independent angiogenesis in adipose tissues during cold acclimation. Cell Metab. *9*, 99–109.

Young, S.G., Fong, L.G., Beigneux, A.P., Allan, C.M., He, C., Jiang, H., Nakajima, K., Meiyappan, M., Birrane, G., and Ploug, M. (2019). GPIHBP1 and lipoprotein lipase, partners in plasma triglyceride metabolism. Cell Metab. *30*, 51–65.

Young, S.G., and Zechner, R. (2013). Biochemistry and pathophysiology of intravascular and intracellular lipolysis. Genes Dev. *27*, 459–484.

Zhang, X., Lam, K.S., Ye, H., Chung, S.K., Zhou, M., Wang, Y., and Xu, A. (2010). Adipose tissue-specific inhibition of hypoxia-inducible factor 1{alpha} induces obesity and glucose intolerance by impeding energy expenditure in mice. J. Biol. Chem. *285*, 32869–32877.

Please cite this article in press as: Fischer et al., Lysosomal lipoprotein processing in endothelial cells stimulates adipose tissue thermogenic adaptation, Cell Metabolism (2020), https://doi.org/10.1016/j.cmet.2020.12.001

STAR★methods

Key resources table

REAGENT or RESOURCE	SOURCE	IDENTIFIER
Antibodies		
Rabbit polyclonal anti-ACC	Cell Signaling	Cat# 3662, RRID:AB_2219400
Rabbit polyclonal anti-AKT	Cell Signaling	Cat#9272; RRID: AB_329827
Hamster monoclonal anti-CD31	Millipore	Cat# MAB1398Z; RRID:AB_94207
Rabbit polyclonal anti-CD36	Moore lab (NYU)	N/A
Rabbit polyclonal anti-DIO_2	Abcam	Cat# ab77779, RRID:AB_1951738
Rabbit monoclonal anti-E-Cadherin	Cell Signaling	Cat# 3195, RRID:AB_2291471
Mouse monoclonal anti-FASN	BD Bioscience	Cat# 610962; RRID:AB_398275
Rat monoclonal anti-GPIHBP1	Young lab (UCLA)	N/A
Rabbit monoclonal anti-HIF1α	Cell Signaling	Cat# 14179; RRID:AB 2622225
Rat monoclonal anti-LAMP2	Santa Cruz Biotechnology	Cat# sc-20004, RRID:AB_626857
Mouse OXPHOS WB cocktail	Abcam	Cat# ab110413, RRID:AB_2629281
Rabbit monoclonal anti-PDK1	Abcam	Cat# ab207450 RRID: N/A
Rabbit monoclonal anti-PLIN1	Cell Signaling	Cat#9349; RRID:AB_10829911
Mouse monoclonal anti-Rab5A	Santa Cruz Biotechnology	Cat# sc-46692; RRID:AB_628191
Rabbit monoclonal anti-gTubulin	Abcam	Cat# ab179503, RRID: N/A
Rabbit anti-UCP1	Cannon lab (Stockholm University)	N/A
Rabbit monoclonal anti-VDAC	Cell Signaling	Cat# 4661; RRID:AB_10557420
Rabbit polyclonal anti-ZO1	Thermo Fisher	Cat# 61-7300, RRID:AB_2533938
Alexa 594 goat-anti-hamster	Jackson ImmunoResearch Labs	Cat# 127-585-099, RRID:AB_2338998
Cy2 donkey-anti-rabbit	Jackson ImmunoResearch Labs	Cat# 711-225-152, RRID:AB_2340612
Cy5 donkey-anti-rat	Jackson ImmunoResearch Labs	Cat# 712-175-153, RRID:AB_2340672
HRP goat anti-mouse	Jackson ImmunoResearch Labs	Cat# 115-035-003, RRID:AB_10015289
HRP goat anti-rabbit	Jackson ImmunoResearch Labs	Cat# 111-035-144, RRID:AB_2307391
HRP goat anti-rat	Jackson ImmunoResearch Labs	Cat# 112-035-175, RRID:AB_2338140
Chemicals and reagents		
Acepromacin	Sigma	Cat# A7111
CD11b MicroBeads	Milteny	Cat# 130-049-601
CD31 MicroBeads	Milteny	Cat# 130-097-418
CL316,243	Tocris	Cat# 1499
Collagenase II	Sigma	Cat# C2-22-BC
cOmplete™ Mini Protease Inhibitor Cocktail	Roche	Cat# 1836153001
DAPI	Invitrogen	Cat# D1306
Dextran40	Sigma	Cat# 68084
DMEM, high glucose	Gibco	Cat# 11965118
Endothelial cell basal media	Promocell	Cat# C-22210
Endothelial cell growth medium SupplementPack	Promocell	Cat# C-39210
Eosin	Merck	Cat# 1.15935
Etomoxir	Sigma	Cat# E1905
EZ-Link NHS-SS-Biotin	Thermo Fisher	Cat# 21441
Hematoxylin	Sigma	Cat# MHS32-1L
Heparin	Rotexmedica	N/A
HIF1α inhibitor (3-(2-(4-Adamantan-1-yl-phenoxy)-acetylamino)-4-hydroxybenzoic acid methyl ester)	Santa Cruz Biotechnology	Cat# sc-205346

(Continued on next page)

Please cite this article in press as: Fischer et al., Lysosomal lipoprotein processing in endothelial cells stimulates adipose tissue thermogenic adaptation, Cell Metabolism (2020), https://doi.org/10.1016/j.cmet.2020.12.001

Continued

REAGENT or RESOURCE	SOURCE	IDENTIFIER
Insulin	Sigma	Cat# I9278
Lalistat2	Cayman Chemical	Cat# 25347
MitoQ	Hölzer	Cat# HY-100116A
NuPAGE LDS 4x sample buffer	Invitrogen	Cat# NP0008
NuPAGE reducing sample buffer	Invitrogen	Cat# NP0004
Pierce Streptavidin Magnetic Beads	Thermo Fisher	Cat# 88817
SolvableTM	Perkin Elmer	Cat# 6NE9100
Scintillation fluid	Zinsser Analytic	Cat# 1008500
Trizol	peqlab	Cat# 30-2010
Western-Type Diet	Sniff	Cat# TD88137 mod
^{3}H-Cholesteryl-hexadecylether	Perkin Elmer	Cat# NET85900
^{3}H-Deoxyglucose	Hartmann Analytik	Cat# MT911
^{3}H-Retinol	Perkin Elmer	Cat# NET927250UC
^{14}C-Triolein	Hartmann Analytik	Cat# ARC 0291
Chromium Single Cell 3′ Library & Gel Bead Kit v3	10x Genomics	Cat# 1000092
Chromium Single Cell 3′ Library Construction Kit v3	10x Genomics	Cat# 1000078
Nuclei EZ Lysis Buffer	Sigma	Cat# NUC101
Critical commercial assays and equipment		
Cy3- CyDye Mono-Reactive Dye Kit	GE Amersham	Cat# GEPA23001
NucleoSpin RNA/Protein kit	Macherey & Nagel	Cat# 740933
High Capacity cDNA RT kit	Invitrogen	Cat# 4368813
Internal Standards Kit for Lipidyzer platform	Sciex	Cat# 5040156
AA 45/32 Phys Control Plasma	Sciex	Cat# 4386703
QC Spike Standards Kit for Lipidyzer platform	Sciex	Cat# 5040408
MACS LD Column	Milteny	Cat# 130-042-401
Quant-iT dsDNA Broad-Range Assay Kit	Invitrogen	Cat# Q33130
Rectal Thermometer	Physitemp	Cat# BAT-12
Thermo Camera	FLIR	Cat# E60
TaqMan assay for *Adipoq*	Thermo Fisher	Mm00456425_m1
TaqMan assay for *Bnip3*	Thermo Fisher	Mm01275601_g1
TaqMan assay for *Cdh5*	Thermo Fisher	Mm00486938_m1
TaqMan assay for *Cd36*	Thermo Fisher	Mm00432403_m1
TaqMan assay for *Cox4i1*	Thermo Fisher	Mm00438289_g1
TaqMan assay for *Cox7a1*	Thermo Fisher	Mm00438297_g1
TaqMan assay for *Cox8b*	Thermo Fisher	Mm00432648_m1
TaqMan assay for *Dio*$_2$	Thermo Fisher	Mm00515664_m1
TaqMan assay for *Elovl3*	Thermo Fisher	Mm00468164_m1
TaqMan assay for *Emr1*	Thermo Fisher	Mm00802530_m1
TaqMan assay for *Fabp4*	Thermo Fisher	Mm00445880_m1
TaqMan assay for *Glut1*	Thermo Fisher	Mm00441480_m1
TaqMan assay for *Glut4*	Thermo Fisher	Mm01245502_m1
TaqMan assay for *Gpihbp1*	Thermo Fisher	Mm01205849_g1
TaqMan assay for *Hilpda*	Thermo Fisher	Mm00727638_s1
TaqMan assay for *Lipa*	Thermo Fisher	Mm00498820_m1
TaqMan assay for *Lipg*	Thermo Fisher	Mm00495368_m1
TaqMan assay for *Lpl*	Thermo Fisher	Mm00434764_m1
TaqMan assay for *Myc*	Thermo Fisher	Mm00487803_m1

(*Continued on next page*)

Please cite this article in press as: Fischer et al., Lysosomal lipoprotein processing in endothelial cells stimulates adipose tissue thermogenic adaptation, Cell Metabolism (2020), https://doi.org/10.1016/j.cmet.2020.12.001

Continued

REAGENT or RESOURCE	SOURCE	IDENTIFIER
TaqMan assay for *Pecam1*	Thermo Fisher	Mm01242584_m1
TaqMan assay for *Pdk1*	Thermo Fisher	Mm00554300_m1
TaqMan assay for *Pdk4*	Thermo Fisher	Mm00443325_m1
TaqMan assay for *Pfkfb 3*	Thermo Fisher	Mm00504650_m1
TaqMan assay for *Pfkfb 4*	Thermo Fisher	Mm00557176_m1
TaqMan assay for *Ppara*	Thermo Fisher	Mm00440939_m1
TaqMan assay for *Pparg*	Thermo Fisher	Mm00440945_m1
TaqMan assay for *Ppargc1a*	Thermo Fisher	Mm00447183_m1
TaqMan assay for *Prdm16*	Thermo Fisher	Mm00712556_m1
TaqMan assay for *Tbp*	Thermo Fisher	Mm00446973_m1
TaqMan assay for *Tjp1*	Thermo Fisher	Mm00493699_m1
TaqMan assay for *Ucp1*	Thermo Fisher	Mm00494069_m1
TaqMan assay for *Vegfa*	Thermo Fisher	Mm00437306_m1
TaqMan assay for *Vegfb*	Thermo Fisher	Mm00442102_m1
TaqMan assay for *Vldlr*	Thermo Fisher	Mm00443281_m1
Experimental models: organisms/strains		
Mouse: C57BL/6J	The Jackson Laboratory	Stock No: 000664
Mouse: B6.129S1-Cd36tm1Mfe/J	The Jackson Laboratory	Stock No: 019006
Mouse: B6.Tg(Cdh5-cre/ERT2)Rha	Eschenhagen lab (UKE)	N/A
Mouse: B6. Lipa^{tm1c}(EUCOMM)Hmgu	Eucomm	ES-cell clone HEPD0960_2_B11
Mouse: B6. Lipa^{tm1c}Hmgu_B6.Tg(Cdh5-cre/ERT2)Rha	This paper	N/A
Mouse: B6.Ucp1-DTReGFP	Wolfrum lab (ETH)	N/A
Cell line: immortalized preadipocytes	Cannon lab (Stockholm)	(Klein et al., 1999)
HUVEC	Promocell	C-12203
Software		
Excel 2018 (Version 16.16.20)	Microsoft	RRID:SCR_016137
GraphPad Prism (Version 8.4.1)	GraphPad	RRID:SCR_002798
Image Studio Lite (Version 5.2.5)	LICOR	RRID:SCR_013715
ImageJ/Fiji	NIH	RRID:SCR_002285
Lipidomics Workflow Manager	SCIEX	RRID:SCR_017003
NIS-Elements Advances Research	NIKON	RRID:SCR_014329
RStudio	RStudio	RRID:SCR_000432
Scrublet		RRID:SCR_018098
Seurat		RRID:SCR_016341

Resource availability

Lead contact

Further information and requests for reagents may be directed to and will be fulfilled by the Lead Contact, Joerg Heeren (heeren@uke.de).

Materials availability

All materials used in this study are either commercially available or through collaboration, as indicated.

Data and code availability

This study did not generate datasets or code. The Single Nucleus RNASeq data analyzed in Figure 2 are reported in detail in (Sun et al., 2020) and sequencing data are deposited in ArrayExpress: E-MTAB-8564 for single-nucleus RNAseq of human BAT cells.

Please cite this article in press as: Fischer et al., Lysosomal lipoprotein processing in endothelial cells stimulates adipose tissue thermogenic adaptation, Cell Metabolism (2020), https://doi.org/10.1016/j.cmet.2020.12.001

Experimental Model and Subject Details

Mice

Experiments were approved by the Animal Welfare Officers of University Medical Center Hamburg-Eppendorf (UKE) and Behörde für Gesundheit und Verbraucherschutz Hamburg. All mice used in this study are listed in the Key Resource Table. For practical reasons, investigators were not blinded as to group allocation. Mice were bred and kept in the animal facility of UKE at room temperature (22-24°C) and a 12-h light, 12-h dark cycle with *ad libitum* access to standard laboratory chow diet and water. The mice used in the studies were C57BL/6J wild type mice (Charles River or bred in-house), *Cd36*$^{-/-}$ mice (Bartelt et al., 2011), as well as *Lipa*$^{fl/fl}$ mice that were crossed with mice carrying the Cdh5-CRE-ERT2 transgene (Tg(Cdh5-cre/ERT2)1Rha (Monvoisin et al., 2006)). For BAT imaging, mice expressing eGFP-labelled diphtheria toxin receptor under control of the Ucp1 promoter (B6.Ucp1-DTReGFP (Rosenwald et al., 2013); kindly provided by Christian Wolfrum, Zurich, Switzerland) were used. To generate *Lipa*$^{fl/fl}$ mice, the *Lipa*$^{tm1a(EUCOMM)Hmgu}$ ES-cell clone HEPD0960_2_B11 was obtained from IMPC/Eucomm consortium (Dickinson et al., 2016). In this clone, the L1L2_Bact_P cassette was inserted at position 34512166 of Chromosome 19 upstream of the critical exon 4. The cassette is composed of an FRT site followed by lacZ sequence and a loxP site. This first loxP site is followed by a neomycin resistance gene under the control of the human beta-actin promoter, SV40 polyA, a second FRT site and a second loxP site. A third loxP site is inserted downstream of the targeted exon at position 34510706. The critical exon is thus flanked by loxP sites. Cells from the clone HEPD0960_2_B11 were injected into C57BL/6J blastocysts to generate chimeras. *Lipa*^{tm1a} mice were genotyped by PCR using *Lipa*-specific primers flanking the 3' loxP site downstream of the critical exon 4 (forward 5'-ATTGACAACAGCAGCTTGGG-3'; reverse 5'-GGGGAGATTGCCTGAGAGTT-3') amplifying PCR products of 403 bp and 480 bp from the wild type and targeted locus, respectively. *Lipa*^{tm1a} mice were backcrossed to C57BL6/J for 7 generations, and heterozygous mice were then crossed with flippase (Flp)-expressing mice to delete the FRT-flanked selection cassette and generate *Lipa*^{tm1c} mice with a floxed exon 4 in the *Lipa* gene. Correct deletion of the FRT-flanked cassette was verified by PCR (forward 5'-GGCCTTTCACTTGCTTGGTT-3'; reverse 5'-GGTTTGCATCGATCCCTGAC-3') yielding products of 443 bp in wild type mice, 646 bp in flipped *Lipa*^{tm1a} mice, and a ~7 kb, and thus undetectable, product in non-flipped *Lipa*^{tm1a} mice. These mice were then crossed with Cdh5-CreERT2-expressing mice to obtain tamoxifen-inducible endothelial cell-specific *Lipa*-deficient mice (*Lipa*$^{fl/fl}$-Cdh5^{Cre+}) and control littermates (*Lipa*$^{fl/fl}$-Cdh5^{Cre-}). Cre-mediated recombination was confirmed by PCR on genomic DNA isolated from brown adipose tissue using the following primers (forward$_{WT+KO}$ 5'-GGCCTTTCACTTGCTTGGT-3, reverse$_{WT}$ 5'-GTTTGCATCGATCCCTGAC, reverse$_{WT+KO}$ 5'-AGCCCACAAGGCCAGGAAT), where the WT-only reverse primer binds in the excised exon, while the WT+KO reverse primer binds in the following intronic sequence, leading to the amplification of two products in tissues without recombination (635 bp and 2053 bp) and one product in tissues with recombination (499 bp).

Routinely, male mice at age 10-18 weeks were used. For high fat diet feeding, mice were fed a cholesterol-enriched high fat diet (Sniff EF R/M acc.TD88137 mod) for 6-8 weeks starting at 6-8 weeks of age. Control mice were housed at room temperature (22°C) or 30°C as indicated. For initial characterization, cold exposure was performed by housing mice at 6°C for 24 hours including a 4-hour fasting period, unless indicated differently. For metabolic studies, tamoxifen treatment of *Lipa*$^{fl/fl}$-Cre mice was performed starting at 6-8 weeks of age by oral gavage of 2 mg tamoxifen in 100 μL corn oil on 3 consecutive days. Subsequently, two different cold exposure regimens were performed. To investigate the functional relevance of endothelial LIPA for BAT function, we set up an experimental design in which BAT is not fully differentiated and the initial thermogenic recruitment response can be captured. To this end, we first acclimated mice to thermoneutrality for 2 weeks to reduce the thermogenic capacity of BAT. Then, mice were housed under cold conditions for 3 days at 18°C and subsequently 4 days at 6°C. To investigate the functional relevance of endothelial LIPA for WAT browning, we kept mice for 4 weeks at room temperature and for additional 4 weeks at 6°C. In the second regimen, mice received another gavage of 2 mg tamoxifen after 2 weeks to account for the appearance of new endothelial cells due to cold-induced angiogenesis (Luo et al., 2017; Xue et al., 2009).

To acutely activate BAT in indirect calorimetry, mice were injected subcutaneously with 1 mg/kg body weight CL316,243, dissolved in sterile saline. For metabolic turnover studies, mice were fasted in single cages for 4 hours prior to injection or gavage of radiolabeled glucose and/or lipids. Blood samples were taken by cardiac puncture in terminally anaesthetized mice. For intravital microscopy, mice were anaesthetized by isoflurane. For all terminal procedures, mice were anesthetized with ketamine (100mg/kg) and xylazine (10mg/kg).

Clinical Studies

The clinical study was approved by the Local Ethics Committee of the University Hospital in Bratislava, Slovakia. All study participants provided witnessed written informed consent prior to entering the study. BAT samples were obtained from the lower third of the neck by an experienced ENT surgeon during neck surgery under general anesthesia. The deep neck BAT samples were taken from pre- and paravertebral space between common carotid and trachea in case of thyroid surgery and just laterally to carotid sheath in case of branchial cleft cyst surgery. Patients with malignant disease and subjects younger than 18 years were excluded from participation in the study. Deep neck BAT samples were collected from 16 individuals (4 male/12 female; 49.2 ± 19.0 years (22 – 77 years); BMI 24.8 ± 4.7 kg/m2 (16.9 – 35.2 kg/m2); body fat 29.1 ± 8.5 % (15.6 – 46.6 %); thyroid surgery n=14 or branchial cleft cyst surgery n=2; data are expressed as mean ± SD. Samples were cleaned immediately from blood and connective tissue, frozen in liquid nitrogen and stored at -80°C.

Please cite this article in press as: Fischer et al., Lysosomal lipoprotein processing in endothelial cells stimulates adipose tissue thermogenic adaptation, Cell Metabolism (2020), https://doi.org/10.1016/j.cmet.2020.12.001

Method Details

Preparation of TRL

Preparation of fluorescently or radioactively labelled TRL was described previously (Bartelt et al., 2011; Heine et al., 2018). Briefly, chloroform lipid extracts from human TRL were traced with [Carboxyl-^{14}C]-triolein and [Cholesteryl-1,2-^{3}H(N)]-cholesteryl hexadecylether. For imaging studies, 10 mg of lipid was mixed with either 0.5 mg super paramagnetic iron-oxide (SPIO) or 40 μl quantum dot (QD) nanocrystals (Chen et al., 2013) per 1 ml of final TRL solution. The solvent was evaporated under nitrogen flow and PBS was added. The mixture was sonicated and filtered through 0.45 μm filters to produce TRL with a diameter typical for postprandial lipoproteins of 250-400 nm (Heine et al., 2018). To produce Cy3-labelled murine TRL, plasma samples were taken from C57BL/6/J mice 2 hours after gavage of 200 μL olive oil. TRL were isolated by ultracentrifugation in a discontinuous KBr gradient. Protein concentration was determined, and 1 mg of protein was labelled with Cy3 using the CyDye Mono-Reactive Dye Kit, according to the manufacturer's instruction. KBr and excess dye were removed by gel filtration through a PD10-column (GE Healthcare). Rat native chylomicrons were prepared as described previously (Hultin et al., 1996). Briefly, primary native rat chylomicrons were isolated from the thoracic duct of anaesthetized rats that had been intragastrically infused with intralipid solution traced with [11,12-^{3}H(N)] retinol and [1-^{14}C] oleic acid.

Metabolic turnover studies

For uptake studies of radiolabeled TRL, mice were fasted for 4 hours before they were intravenously injected with 200 μl of TRL-solution (80 mg triglyceride/kg body weight), traced with ^{3}H-cholesteryl ether (0.15 – 0.75 MBq/kg body weight) and ^{14}C-triolein (0.03 – 0.15 MBq/kg body weight) (Heine et al., 2018). Alternatively, mice were injected with tracer doses of ^{3}H-deoxyglucose and a TRL-solution containing ^{14}C-triolein. For oral glucose and fat tolerance tests (OGFT), mice were fasted for 4 hours before receiving an oral gavage of 300 μl of a glucose-lipid-emulsion containing 47 mg/kg body weight triglycerides from intralipid and 2 g/kg body weight glucose, traced with ^{3}H-deoxyglucose (0.72 MBq/kg body weight) and ^{14}C-triolein (0.15 MBq/kg body weight). After 20 minutes (TRL turnover) or 2 hours (OGFT), mice were anaesthetized and transcardially perfused with PBS containing 10 U/ml heparin. For heparin-release studies, mice were injected rat chylomicrons double-labeled with ^{3}H-retinylester and ^{14}C-triolein in combination with injection of 100 U heparin or vehicle at indicated time points. Organs were harvested and dissolved in 10x (v/w) Solvable™, and radioactivity (in dpm) was measured by scintillation counting using a Perkin Elmer Tricarb Scintillation Counter. Radioactive uptake into different cells in BAT was measured by liquid scintillation counting on cell fractions, isolated as described below.

Isolation of endothelial cells, tissue-resident macrophages and brown adipocytes

Dissected and pooled interscapular BAT or inguinal WAT were minced with surgical scissors, and digested for 45 min at 37°C in PBS containing 10 mM $CaCl_2$, 2.4 units/mL dispase II, and 1.5 units/mL collagenase D. After digestion, the homogenate was passed through a cell strainer (100 μm), and the flow through was centrifuged for 5 min, at 600 x g, 4°C. The pellet was resuspended in PBS containing 2 mM EDTA, 0.5% BSA, 2 mM glucose, and filtered through a cell strainer (40 μm). The filtrate was centrifuged at 600 x g for 5 min, the cell pellet was resuspended and incubated with CD11b MicroBeads for depletion or isolation of the macrophage fraction (Miltenyi; 10 μl beads/10^7 cells). CD11b$^+$ cells were captured from the lysate using magnetic columns (Miltenyi). The flow through was centrifuged, the pellet was resuspended and incubated with CD31 MicroBeads (Miltenyi; 10 μl beads/10^7 cells) to isolate endothelial cells. The flow through, containing predominantly adipocytes, was collected. Cell fraction pellets were then dissolved either in TRIzol® reagent for RNA extraction, liquid scintillator for radioactivity counting or in PBS for DNA quantification.

Immunofluorescence, transmission electron microscopy and HE-staining

To follow the fate of lipoproteins into activated BAT, mice were injected intravenously with 200 μl Cy3-labeled murine chylomicrons or quantum dot (QD)-labelled TRL. After 15 min, mice were anesthetized with ketamin/rompun and perfused transcardially with ice-cold PBS containing 4% paraformaldehyde and 5% sucrose for 2 min at constant perfusion rate (5 ml/min). Afterwards, BAT was harvested, post-fixed for 1 hour, embedded in gelatin, and cut into 200 μm slices using a vibratome (Leica). Background fluorescence was reduced by incubation with 5% glycine in PBS for 30 min. Afterwards, sections were then permeabilized and blocked in 3% BSA, 0.1% Triton-X-100 for 1 hour at room temperature. Primary antibody incubation was performed in 3% BSA in PBS at 4°C over night. The following primary antibodies were used: rat-anti-GPIHBP1 (1:500), hamster-anti-CD31(1:250), rabbit-anti-CD36 (1:1000) or rabbit-anti-Perilipin (1:1000). Sections were then washed 3 times 10 min with PBS and incubated for 1 hour at room temperature with the following secondary antibodies in 3% BSA: Alexa 594 goat-anti-hamster (1:500); Cy2-donkey-anti-rabbit (1:500); Cy5-donkey-anti-rat (1:250). Subsequently, sections were again washed 3 times, nuclei were stained with DAPI, and fluorescent microscopy was performed on a NikonA1 Ti confocal laser scanning microscope as described before (Fischer et al., 2019).

Quantification of CD31 was performed using the ImageJ channel quant function. For this, the fluorescence intensity of three independent BAT images per mouse were quantified, and normalized to total image area.

For transmission electron microscopy, mice were injected intravenously with 200 μL SPIO-labeled TRL. After 30 min, mice were sacrificed with a lethal dose of ketamin/rompun injection anesthesia and perfused with PBS containing 2% paraformaldehyde and 1% glutaraldehyde for 2 min (5 mL/min). Then, interscapular BAT was dissected and prepared for electron microscopy by the Tokuyasu technique. 70 nm ultra-thin sections were examined with a FEI Tecnai G20 transmission electron microscope operated at 80 kV.

Please cite this article in press as: Fischer et al., Lysosomal lipoprotein processing in endothelial cells stimulates adipose tissue thermogenic adaptation, Cell Metabolism (2020), https://doi.org/10.1016/j.cmet.2020.12.001

Hematoxylin-Eosin stainings were performed on paraffin-embedded tissues using standard procedures (Fischer et al., 2019). Images were taken using a NikonA1 Ti microscope equipped with a DS-Fi-U3 brightfield camera.

Intravital microscopy and magnetic resonance imaging

Intravital microscopy was performed as described previously (Heine et al., 2018). Briefly, mice were anaesthetized with isoflurane inhalation anesthesia and interscapular BAT was surgically prepared. BAT was visualized using a NikonA1 Ti confocal laser scanning microscope, equipped with a fast resonance scanner at 30 fps. 200 µl of QD-labelled TRL were injected via a tail vein catheter, and the uptake of QD-TRL was monitored for 10 min. BAT structure was visualized using a 648 nm laser combined with a 648 nm detector in reflection mode.

Dynamic non-invasive magnetic resonance imaging (MRI) was performed as described before (Bruns et al., 2009; Heine et al., 2018). Briefly, anesthetized mice were injected with 200 µl of SPIO-labelled TRL without or in combination with 100 U heparin at indicated time points. MRI scanning was performed with a 3 Tesla clinical MR scanner (Philips Medical Systems, the Netherlands) equipped with a custom-made small animal solenoid coil. The scan protocol included a T2*-weighted imaging, which is highly sensitive to susceptibility effects caused by local magnetic field inhomogeneities indicating SPIO presence. Quantification of the SPIO-induced negative contrast was performed in ImageJ using a ROI covering interscapular BAT.

In vivo biotinylation

For *in vivo* biotinylation (Fischer et al., 2018a), mice were injected intraperitoneally with acepromazin (3 mg/kg body weight) to promote vasodilatation. Immediately afterwards, mice were anesthetized with ketamin/rompun and perfused with 10 mL PBS containing 10% (w/v) Dextran40. Afterwards mice were perfused with a biotinylation solution containing 1 mg/mL EZ-Link NHS-SS-Biotin in perfusion buffer for 10 min at a constant perfusion rate (1.5 mL/min). For quenching of unreacted biotin, mice were further perfused with 10 mL quenching solution (50 mM Tris-HCl in 10% Dextran40/PBS; pH 7.4). Interscapular BAT was dissected and lysed in cell lysis buffer (pH 8,0) supplemented with 50 mM Tris base, 2 mM $CaCl_2$, 80 mM NaCl, 1% Triton X-100 and Complete mini protease inhibitor cocktail using the TissueLyser (Qiagen). After centrifugation (14000 rpm, 4°C), the biotinylated protein containing supernatant was incubated with pre-washed Pierce™ streptavidin magnetic beads according to the manufacturer's instructions. After incubation at 4°C for 1.5 hours on a rotating wheel, magnetic beads were washed with TBST followed by PBS. Biotinylated proteins were eluted in NuPAGE reducing sample buffer and subjected to Western blotting (see below).

Magnetic organelle isolation

To isolate organelles from BAT of cold-activated mice, mice were exposed to 6°C for 24 hours and injected with 200 µl SPIO-TRL or QD-TRL, as described above. 15 min after injection, the mice were anaesthetized and transcardially perfused with PBS containing 10 U/ml heparin. BAT was harvested, placed in ice-cold 250 mM sucrose solution, minced with scissors and homogenized with 8 strokes using a glass potter homogenizer. Lysates were filtered through a 100 µm cell strainer and centrifuged at 800 g for 10 min to obtain a postnuclear supernatant. The supernatant, without the top fat layer, was harvested and centrifuged again to avoid lipid contamination. The resulting supernatant was filtered again through a 30 µm cell strainer and applied on magnetic separation columns (Miltenyi). The columns were washed with 250 mM sucrose, the bound fraction was eluted in PBS, and proteins were precipitated using pure trichloroacetic acid (TCA). The pellet was washed with acetone, dried and resuspended in NuPAGE reducing sample buffer for Western blot analysis (see below).

Cell culture

Immortalized brown adipocyte precursors (Klein et al., 1999) were cultured in DMEM/high glucose supplemented with 10% FBS (Gemini Benchmark) and 1% Penicillin/Streptavidin. HUVEC cells were cultured in endothelial cell media supplemented with the recommended Supplement Pack (Promocell). Cells were cultured in the presence of either Lalistat2 (30 µM), HIF1α inhibitor 3-(2-(4-Adamantan-1-yl-phenoxy)-acetylamino)-4-hydroxybenzoic acid methyl ester (30 µM), Etomoxir (100 µM), MitoQ (100 nM) or vehicle (DMSO), and treated with TRL (25 µg/ml) as indicated in the figure legend. For determining proliferation, ^{3}H-thymidine (0.1 mCi per ml) was added to the cells for 3 hours before harvesting the cells. Cellular DNA was precipitated and washed with 10% TCA. Afterwards, DNA was dissolved in 0.2 M NaOH, and radioactivity was measured by scintillation counting. Stromal-vascular fractions from BAT were isolated from male wildtype C57BL/6J mice aged 4-6 weeks and brown adipocyte differentiation was induced as described (Fischer et al., 2019). The differentiation protocol was conducted in the absence or presence TRL or LDL (25 µg/ml), Lalistat2 (30 µM), HIF1α inhibitor (30 µM), MitoQ (100 µM) or vehicle (DMSO) as indicated in the figure legend. Ultimately, cells were washed with PBS and harvested either in Trizol or RIPA buffer.

Western blotting

Western blotting was performed using standard procedures (Fischer et al., 2019). Primary antibodies (in 5% BSA in TBS-T) were applied over night at 4 °C. Secondary antibodies were diluted 1:5000 in 5% milk powder in TBS-T, and detection was performed with enhanced chemiluminescence using Amersham Hyperfilm (GE Healthcare) or Amersham Imager 600 (GE Healthcare). The following primary antibodies were used: rabbit-anti-ACC (1:1000; Cell Signaling), rabbit-anti-AKT (1:1000; Cell Signaling), rabbit-anti-CD36 (1:5000), rabbit-anti-DIO_2 (1:1000; Abcam), rabbit-anti-E-Cadherin (1:1000, Cell Signaling), mouse-anti-FASN (1:500; BD Biosciences), rat-anti-GPIHBP1 (1:400), rabbit-anti-HIF1a (1:1000; Cell Signaling), rat-anti-LAMP2 (1:200; Santa Cruz Biotech-

Please cite this article in press as: Fischer et al., Lysosomal lipoprotein processing in endothelial cells stimulates adipose tissue thermogenic adaptation, Cell Metabolism (2020), https://doi.org/10.1016/j.cmet.2020.12.001

nology), mouse-anti-OXPHOS (1:20000; Abcam ab110413), rabbit-anti-PDK1 (1:1000; Abcam); mouse-anti-Rab5 (1:250; Santa Cruz Biotechnology), rabbit-anti-gTubulin (1:2000, Abcam), rabbit-anti-UCP1 (1:25.000 for BAT and 1:5000 for iWAT), rabbit-anti-VDAC (1:1000; Cell Signaling), rabbit-anti-ZO1 (1:1000, Invitrogen). Quantification was performed using ImageStudio Lite (Licor). For calculation of BAT and inguinal WAT total UCP1 and OXPHOS levels, the expression levels as measured by Western blot were multiplied with the tissue total protein content.

Indirect calorimetry

For measurement of metabolic activity, mice were transferred to IVC green line cages in a TSE PhenoMaster system in a temperature- and humidity-controlled cabinet. The mice were allowed to acclimate to the chambers for 1 day at indicated temperatures. Oxygen consumption, carbon dioxide production, as well as energy (calculated from food intake) and water intake and locomotor activity were monitored continuously in 15-21 min intervals. The cabinets were kept at 6°C for cold-acclimated and acutely cold-exposed mice. For measurement of maximal adaptive thermogenic capacity, cold-acclimated mice were kept in the TSE system at 28°C for 1 day and then injected with 1 mg/kg CL316,243 (Fischer et al., 2017; Heine et al., 2018). Energy expenditure (in Watt) was calculated using a modified Weir equation (Fischer et al., 2018b), and RQ was calculated as $V(CO_2)/V(O_2)$.

Measurement of heat-loss and body temperature

Body temperature in cold-acclimated mice was measured using a rectal probe (Physitemp BAT-12), inserted 1 cm into the rectum. Tail heat loss was measured as described previously (Fischer et al., 2016) using a FLIR E60 thermal camera (FLIR, Germany).

Gene expression Analysis of murine samples

Total RNA was isolated from cell samples or whole tissue using the NucleoSpin RNA II kit (Macherey & Nagel). After synthesis of cDNA, quantitative real-time PCR was performed and relative expression of genes of interest was calculated by normalization to housekeeper TATA-box binding protein (*Tbp*) mRNA using the $2^{-\Delta\Delta Ct}$ method.

RNAseq of human BAT samples

Nuclei were isolated following a modified nuclear isolation protocol. (https://doi.org/10.1101/2020.01.20.890327). Briefly, frozen human BAT tissue were thawed on ice, minced to 1 mm3 and homogenized in cold 0.1% CHAPS in Tris-HCL. The minced adipose tissue was filtered through 40 μm cell strainer, centrifuged at 500 xg for 5 minutes at 4°C and the pellet was resuspended in PBS with DAPI. Nuclei suspensions were loaded to MoFlo Astrios EQ Cell Sorter and sorted into a 1.5 ml tube. 10x based libraries were acquired with Chromium Single Cell V3.0 reagent kit following manufacturer's protocol (10x Genomics). Nuclei suspensions containing at ~500 nuclei/μl were loaded to nine independent lanes. Libraries were sequenced on a Novaseq 6000 (Illumina). For data analysis, first we applied CellBender (https://www.biorxiv.org/content/10.1101/791699v1) to distinguish cell-containing droplets from empty droplets. Then, we applied Scrublet (Wolock et al., 2019), DoubletFinder (McGinnis et al., 2019) to exclude potential doublets, while nuclei that express both male and female signature genes were excluded for down-stream analysis. Human Ensembl-GRCh38.p13 was used for mapping. CCA (Stuart et al., 2019) from Seurat package was applied for batch correcting, clustering and signature genes identification. SingleR was applied for annotation (Aran et al., 2019).

Lipidomic analysis using MS/MS approach

For lipidomic analysis, sample preparation and analysis were performed according to protocols of the Lipidyzer™ Platform using the corresponding standard kits (SCIEX). Briefly, 5 mg of snap frozen interscapular BAT and inguinal WAT were homogenized and extracted using a MTBE/methanol extraction. Lipidyzer™ Internal Standards (SCIEX) were added to all samples during lipid extraction. Lipid extracts were concentrated and reconstituted in running buffer (10mM ammonium actetate, dichloromethane (50): methanol (50)). Quantitative measurement of lipid species was performed using an ESI-QqQ system in multiple reaction monitoring (MRM) mode (QTRAP® 5500; SCIEX)). Quantification of lipids was conducted by the Lipidyzer™ software was used (Lipidomics Workflow Manager software; SCIEX).

Quantification and statistical analysis

Data are expressed as mean ± S.E.M. Two groups were compared by Student's t test, more than two groups by ANOVA followed by Sidak's or Tukey's correction for multiple comparison. No method was used to determine whether the data met assumptions of either Student's t test or ANOVA. The statistical parameters (i.e. p values, numbers of biological repeats) can be found in the figure legends. No exclusion or inclusion criteria were used for data analyses. Microsoft Excel 2016 and GraphPad Prism 6.0 were used for statistical calculations. $P \leq 0.05$ was considered to be statistically significant.